



UNIVERSIDAD DE INVESTIGACIÓN DE TECNOLOGÍA EXPERIMENTAL YACHAY TECH

Escuela de Ciencias Químicas e Ingenierías

TÍTULO: A NOVEL HYDROGEN PEROXIDE SENSOR BASED ON GRAPHITE ELECTRODE MODIFIED BY MULTIWALLED CARBON NANOTUBES DOPED WITH HYDROXYAPATITE NANOPARTICLES

Trabajo de integración curricular presentado como requisito para la
obtención del título de QUÍMICO/A

Autor:

Moreno Barreno Andrés David

Tutor:

Ph.D. Díaz Barrios Antonio

Urcuquí, Agosto 2019

Urcuquí, 30 de agosto de 2019

SECRETARÍA GENERAL
(Vicerrectorado Académico/Cancillería)
ESCUELA DE CIENCIAS QUÍMICAS E INGENIERÍA
CARRERA DE QUÍMICA
ACTA DE DEFENSA No. UITEY-CHE-2019-00010-AD

En la ciudad de San Miguel de Urcuquí, Provincia de Imbabura, a los 30 días del mes de agosto de 2019, a las 15:00 horas, en el Aula AI-102 de la Universidad de Investigación de Tecnología Experimental Yachay y ante el Tribunal Calificador, integrado por los docentes:

Presidente Tribunal de Defensa	Dra. GONZALEZ VASQUEZ, GEMA , Ph.D.
Miembro No Tutor	Dr. SAUCEDO VAZQUEZ, JUAN PABLO , Ph.D.
Tutor	Dr. DÍAZ BARRIOS, ANTONIO , Ph.D.

Se presenta el(la) señor(ita) estudiante **MORENO BARRENO, ANDRES DAVID**, con cédula de identidad No. **0603399031**, de la **ESCUELA DE CIENCIAS QUÍMICAS E INGENIERÍA**, de la Carrera de **QUÍMICA**, aprobada por el Consejo de Educación Superior (CES), mediante Resolución RPC-SO-39-No.456-2014, con el objeto de rendir la sustentación de su trabajo de titulación denominado: **A NOVEL HYDROGEN PEROXIDE SENSOR BASED ON GRAPHITE ELECTRODE MODIFIED BY MULTIWALLED CARBON NANOTUBES DOPED WITH HYDROXYAPATITE NANOPARTICLES**, previa a la obtención del título de **QUÍMICO/A**.

El citado trabajo de titulación, fue debidamente aprobado por el(los) docente(s):

Tutor	Dr. DÍAZ BARRIOS, ANTONIO , Ph.D.
--------------	-----------------------------------

Y recibió las observaciones de los otros miembros del Tribunal Calificador, las mismas que han sido incorporadas por el(la) estudiante.

Previamente cumplidos los requisitos legales y reglamentarios, el trabajo de titulación fue sustentado por el(la) estudiante y examinado por los miembros del Tribunal Calificador. Escuchada la sustentación del trabajo de titulación, que integró la exposición de el(la) estudiante sobre el contenido de la misma y las preguntas formuladas por los miembros del Tribunal, se califica la sustentación del trabajo de titulación con las siguientes calificaciones:

Tipo	Docente	Calificación
Tutor	Dr. DÍAZ BARRIOS, ANTONIO , Ph.D.	9,5
Miembro Tribunal De Defensa	Dr. SAUCEDO VAZQUEZ, JUAN PABLO , Ph.D.	9,2
Presidente Tribunal De Defensa	Dra. GONZALEZ VASQUEZ, GEMA , Ph.D.	9,4

Lo que da un promedio de: **9.3 (Nueve punto Tres)**, sobre 10 (diez), equivalente a: **APROBADO**

Para constancia de lo actuado, firman los miembros del Tribunal Calificador, el/la estudiante y el/la secretario ad-hoc.


MORENO BARRENO, ANDRES DAVID
Estudiante

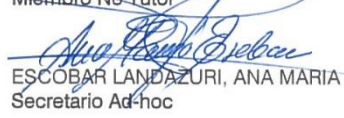

Dra. GONZALEZ VASQUEZ, GEMA , Ph.D.
Presidente Tribunal de Defensa


Dr. DÍAZ BARRIOS, ANTONIO , Ph.D.
Tutor





Dr. SAUCEDO VAZQUEZ, JUAN PABLO , Ph.D.
Miembro No Tutor



ESCOBAR LANDAZURI, ANA MARIA
Secretario Ad-hoc



AUTORÍA

Yo, **ANDRÉS DAVID MORENO BARRENO**, con cédula de identidad **0603399031**, declaro que las ideas, juicios, valoraciones, interpretaciones, consultas bibliográficas, definiciones y conceptualizaciones expuestas en el presente trabajo; así cómo, los procedimientos y herramientas utilizadas en la investigación, son de absoluta responsabilidad de el/la autora (a) del trabajo de integración curricular. Así mismo, me acojo a los reglamentos internos de la Universidad de Investigación de Tecnología Experimental Yachay.

Urcuquí, Agosto 2019.

Andrés David Moreno Barreno

CI: 0603399031

AUTORIZACIÓN DE PUBLICACIÓN

Yo, **ANDRÉS DAVID MORENO BARRENO**, con cédula de identidad **0603399031**, cedo a la Universidad de Tecnología Experimental Yachay, los derechos de publicación de la presente obra, sin que deba haber un reconocimiento económico por este concepto. Declaro además que el texto del presente trabajo de titulación no podrá ser cedido a ninguna empresa editorial para su publicación u otros fines, sin contar previamente con la autorización escrita de la Universidad.

Asimismo, autorizo a la Universidad que realice la digitalización y publicación de este trabajo de integración curricular en el repositorio virtual, de conformidad a lo dispuesto en el Art. 144 de la Ley Orgánica de Educación Superior

Urcuquí, Agosto 2019.

Andrés David Moreno Barreno

CI: 0603399031

Dedicatoria

Dedico esta tesis a DIOS, a Santo Tomás de Aquino, patrón de los estudiantes y a la Virgen María, quien inspiró mi espíritu para la conclusión de esta tesis. A mi madre, que nunca dejó de creer en mí y siempre me demostró su amor constante. A mis hermanos, que me han enseñado el valor de la familia. A mi padre, quien a pesar de no estar en este mundo, siempre me cuidó y me dio fuerzas del cielo para continuar mis estudios. Finalmente, a mi gran amigo y tutor Antonio Díaz, porque sin su ayuda nunca podría haber realizado esta tesis. Les agradezco a todos desde el fondo de mi alma. Para todos ellos hago esta dedicación.

Andrés David Moreno Barreno

Agradecimiento

La investigación que condujo a estos resultados recibió financiación de CEDIA (Corporación Ecuatoriana para el Desarrollo de la Investigación y la Academia) a través del proyecto "Biosensores detectados en nanotubos de carbono modificados para la detección de enzimas", bajo el código del acuerdo de subvención: CEPRA XII-2018 -14, Biosensores. La primera parte del proyecto se llevó a cabo bajo la supervisión de Antonio Díaz, Ph.D., Gottfried Suppan, Ph.D. en Urcuquí en los laboratorios de Química E2-E3 de la Universidad Yachay Tech y la segunda parte se realizó bajo la supervisión de Lenys Hernández, Ph.D., y Patricio Espinoza, Ph.D., en Quito en los laboratorios de Química Analítica de la Pontificia Universidad Católica del Ecuador (PUCE). Los nanomateriales de carbono utilizados para esta tesis fueron donados por Ph.D. Gema González, profesora de la escuela de Ciencias Físicas y Nanotecnología de la Universidad Tecnológica de Yachay. A todos los docentes mencionados agradezco por su apoyo incondicional y a quienes felicito por su profesionalismo, digno de admiración.

Andrés David Moreno Barreno

Resumen

Se preparó con éxito un nuevo sensor electroquímico que es simple, económico, confiable y altamente sensible para la detección de peróxido de hidrógeno (H_2O_2) basado en azul de Prusia (PB) y nanotubos de carbono multi-pared (MWCNT siglas en inglés) dopados con nanopartículas de hidroxiapatita (HAp). Los rendimientos electroquímicos del sensor desarrollado se caracterizaron por voltametría cíclica (CV) y cronoamperometría, utilizando $[\text{Fe}(\text{CN})_6]^{3-/4-}$ como sistema redox de referencia y $0,1 \text{ mol L}^{-1}$ PBS con $\text{pH} = 7,4$ como electrolito de soporte para este experimento. Los voltamogramas cíclicos revelaron la actividad electrocatalítica del PB hacia la reducción del peróxido de hidrógeno. Una dependencia lineal de la concentración de H_2O_2 de 1 mM a 10 mM ($R = 0,9763$), con una sensibilidad de detección de $119 \mu\text{A mM}^{-1}\text{cm}^{-2}$. Este trabajo demuestra la viabilidad del auto-ensamblado de electrodos para construir un sensor de H_2O_2 , y también evidencia el gran potencial de los nanomateriales de carbono, como los CNT dopados con nanopartículas inorgánicas para la construcción de dispositivos bioelectrónicos y biosensores. Las respuestas del sensor en rangos de concentración más bajos aún están en estudio y muestran resultados prometedores.

Palabras Clave:

Azul de Prusia, nanopartículas de hidroxiapatita, sensor electroquímico, peróxido de hidrógeno.

Abstract

A new electrochemical sensor that is simple, economic, reliable and highly sensitive for detection of hydrogen peroxide (H_2O_2) based on Prussian Blue (PB) and multiwalled carbon nanotubes (MWCNTs) doped with hydroxyapatite nanoparticles (HAp) was successfully prepared. The electrochemical performances of the developed sensor were characterized by cyclic voltammetry (CV) and chronoamperometry, using $[\text{Fe}(\text{CN})_6]^{3-/4-}$ as benchmark redox system and 0.1 mol L^{-1} PBS with $\text{pH} = 7.4$ was probed as the optimal supporting electrolyte for this experiment. Cyclic voltammograms revealed the electrocatalytic activity of the PB toward reduction of hydrogen peroxide. A linear dependence on H_2O_2 concentration from 1 mM to 10 mM ($R = 0.9763$), with a detection sensitivity of $119\text{ }\mu\text{A mM}^{-1}\text{cm}^{-2}$. This work demonstrates the feasibility of self-assembled of electrode to build up a H_2O_2 sensor, and also evidence the great potential of carbon nanomaterials, such as CNTs doped with inorganic nanoparticles for constructing of bioelectronics devices and biosensors. The sensor's responses at lower concentration ranges is still under study and shows promising results.

Keywords:

Prussian blue, hydroxyapatite nanoparticles, electrochemical sensor, hydrogen peroxide.

CONTENTS

	PAGE
CONTENTS.....	I
CHAPTER 1 PURPOSE AND SIGNIFICANCE OF THIS STUDY	1
1.1 INTRODUCTION	1
1.2 GENERAL OBJECTIVE	2
1.2.1 <i>Specific Objectives</i>	2
CHAPTER 2 LITERATURE REVIEW.....	3
2.1 SENSORS.....	3
2.1.1 CLASSIFICATION OF SENSORS	4
2.1.1.1 <i>Optic Sensor</i>	4
2.1.1.2 <i>Mass-Based Sensor</i>	5
2.1.1.3 <i>Electrochemical Sensor</i>	5
2.2 CARBON NANOTUBES.....	7
2.2.1 HYDROXYAPATITE	10
2.3 PRUSSIAN BLUE	11
2.3.1 ELECTROCHEMISTRY PROPERTIES OF PRUSSIAN BLUE	12
2.4 ELECTROCHEMICAL SENSING OF HYDROGEN PEROXIDE.....	13
CHAPTER 3 EXPERIMENTAL.....	14
3.1 TECHNIQUES OF CHARACTERIZATION.....	14
3.1.1 CYCLIC VOLTAMMETRY.....	14
3.1.1.2 <i>Characteristic Parameters of a Cyclic Voltammogram</i>	15
3.1.2 CHRONOAMPEROMETRY.....	17
3.2 ELECTRODES AND ELECTROCHEMICAL CELL.....	18
3.2.1 WORKING ELECTRODE (WE).....	18
3.2.2 REFERENCE ELECTRODE (RE)	18
3.2.3 COUNTER ELECTRODE (CE)	18
3.3 REAGENTS AND SOLUTIONS	19
3.4 INSTRUMENTATION	20

3.5 GRAPHITE ELECTRODE MANUFACTURE	21
3.6 PREPARATION AND CHARACTERIZATION OF MODIFIED ELECTRODES....	23
3.7 ELECTRODEPOSITION OF PRUSSIAN BLUE	23
CHAPTER 4 RESULTS AND DISCUSSION	25
4.1 CHARACTERIZATION OF CARBON NANOTUBES (CNT)	25
4.1.1 FOURIER TRANSFORMED INFRARED SPECTROSCOPY (FTIR).....	25
4.1.2 X-RAY DIFFRACTION (XRD).....	27
4.1.3 TRANSMISSION ELECTRON MICROSCOPY (TEM).....	28
4.2 CHARACTERIZATION OF PURE HYDROXYAPATITE (HAP)	29
4.2.1 FOURIER TRANSFORMED INFRARED SPECTROSCOPY (FTIR).....	29
4.2.2 X-RAY DIFFRACTION (XRD).....	30
4.2.3 TRANSMISSION ELECTRON MICROSCOPY (TEM).....	32
4.3 CHARACTERIZATION OF NANOSTRUCTURED SYSTEMS WITH HYDROXYAPATITE (CNT/HAP)	33
4.3.1 FOURIER TRANSFORMED INFRARED SPECTROSCOPY (FTIR).....	33
4.3.2 X-RAY DIFFRACTION (XRD).....	35
4.3.3 TRANSMISSION ELECTRON MICROSCOPY (TEM).....	35
4.4 ELECTROCHEMICAL CHARACTERIZATION	37
4.4.1 ELECTROCHEMICAL BEHAVIOR OF 2H-GE ELECTRODE	38
4.4.2 ELECTROCHEMICAL BEHAVIOR OF MODIFIED ELECTRODES.....	41
4.4.3 ELECTROCHEMICAL BEHAVIOR OF PRUSSIAN BLUE FILM	46
4.5 STABILIZATION OF ELECTROCHEMICAL SENSOR	48
4.6 RESPONSE OF THE MODIFIED ELECTRODES TO H₂O₂.....	50
4.7 VOLTAMMETRIC DETECTION OF HYDROGEN PEROXIDE.....	51
CHAPTER 5 CONCLUSIONS	56
REFERENCES	57

LIST OF TABLES

Acronyms & Abbreviations	VI
Table 1. Theoretical and experimentally measured properties of carbon nanotubes.	9
Table 2. Characteristic DRX data of hexagonal graphite.	28
Table 3. Diameter of the CNT obtained in the different steps of the functionalization process.	29
Table 4. Reflections observed in XRD of stoichiometric hydroxyapatite.....	31
Table 5. FTIR bands of the HAp and the CNT _f / HAp (36) and CNT _f / HAp (100) systems.	34
Table 6. Electrochemical parameters obtained from cyclic voltammogram of 2H graphite electrode of 4 mM K ₃ [Fe (CN) ₆] containing in 0.1 M PBS, at different scan rates.	39
Table 7. Electrochemical parameters obtained from cyclic voltammogram of 2H graphite electrode modified with MWCNTs and HAp-MWCNTs of 4mM K ₃ [Fe (CN) ₆] containing in 0.1 M PBS, at different scan rates.	46

LIST OF FIGURES

Figure 1. Diagram representing an electrochemical sensor.	4
Figure 2. Classification of biosensors based on the transducer element and bio-recognition element	6
Figure 3. The waveform of the potential applied during a typical cyclic voltammetry experiment	14
Figure 4. A typical cyclic voltammogram	15
Figure 5. Chronoamperometry	17
Figure 6. Design of electrochemical cell.....	21
Figure 7. Construction of 2H-graphite electrode.....	22
Figure 8. Scheme of experimental procedure.....	24
Figure 9. Scheme of assembly of electrochemical sensor.	24
Figure 10. FTIR spectrums of CNTs of 400 to 4000cm ⁻¹	26
Figure 11. FTIR spectrums of CNTs of 400 to 1800cm ⁻¹	26
Figure 12. DRX patterns of: a) pristine CNTs, b) CNT _p B, c) CNT _f B and d) CNT _f A.	27
Figure 13. CNT TEM images: a) Pristine CNTs, b) CNT _p , c) CNT _f -B, d) CNT _f -A.	28
Figure 14. FTIR spectrum of synthesized HAp.	29
Figure 15. Diffractogram of the synthesized HAp	30
Figure 16. TEM image of the synthesized HAp.	33
Figure 17. FTIR spectra of CNT _f / HAp nanostructured systems	34
Figure 18. XRD standards of the CNT _f / HAp nanostructured compounds.....	35
Figure 19. TEM-HR images of the CNT _f / HAp nanostructured system (36).	36
Figure 20. TEM-HR images of the CNT _f / HAp nanostructured system (100).	36
Figure 21. Cyclic voltammogram of bare and modified electrodes in 0.1 mol L ⁻¹ PBS, at scan rate of 100 mV s ⁻¹	37
Figure 22. Cyclic voltammograms of 2H-GE recorded in 4mM K ₃ [Fe (CN) ₆] with phosphate buffer solution (pH = 7.4) at different scan rates	38
Figure 23. A) Plot of anodic and cathodic peak current and square root of scan rate, and B) Linear relationship of log (anodic current, ip _a) with the log (scan rate) for 2H graphite electrode unmodified.	40

- Figure 24.** Cyclic voltammograms of 2Hgraphite electrode modified with A) MWCNTs and B) HAp-MWCNTs, immersed in 4 mM $K_3 [Fe(CN)_6]$ solution with 0.1 M PBS (pH 7.4).42
- Figure 25.** Cyclic Voltammograms of various electrodes immersed in 4 mmol L^{-1} $[Fe (CN)_6]^{3-/4-}$ with 0.1 mol L^{-1} PBS recorded on a) bare 2H-GE, b) 2H-GE/HAp-MWCNTs, and c) 2H-GE/MWCNTs, at scan rate of 100 mVs^{-1}43
- Figure 26.** Plots: peak currents of 2H-GE/MWCNTs vs. a) square root of scan rate, b) log (scan rate), and peaks currents of 2H-GE/HAp-MWCNTs vs. c) square root of scan rate, d) log (scan rate).44
- Figure 27.** Cyclic voltammograms of Prussian Blue films activated in 0.1 M HCl + 0.1 M KCl solution on modified graphite electrode with A) MWCNTs, and B) HAp-MWCNTs.47
- Figure 28.** Cyclic voltammograms showing the current responses of A) MWCNTs/PB, and B) HAp-MWCNTs/PB modified electrodes in 0.1 M PBS, at alkaline pH of 7.4, at different scan rates.49
- Figure 29.** Cyclic Voltammograms of 2H-GE modified by a) HAp-MWCNTs, b) MWCNTs, c) MWCNTs/PB and c) HAp-MWCNTs/PB in 0.1 M PBS in 1mM H_2O_2 , at pH 7.4. Scan rate of 50 mVs^{-1}51
- Figure 30.** Voltammetric response of 1.0-10mM H_2O_2 at MWCNTs/PB modified electrode, at scan rate of 50 $mV s^{-1}$. Inset: Plot of response current versus H_2O_2 concentration.52
- Figure 31.** Voltammetric response of 1.0-10mM H_2O_2 at HAp-MWCNTs/PB modified electrode, at scan rate of 50 $mV s^{-1}$. Inset: Plot of response current versus H_2O_2 concentration.53

Acronyms & Abbreviations

<i>Abbreviations</i>	<i>Meaning</i>
CNTs	Carbon nanotubes
MWCNTs	Multi-walled carbon nanotubes
SWCNTs	Single-walled carbon nanotubes
GE	Graphite electrode
CPG	Composite pencil graphite
PB	Prussian Blue
HAp	Hydroxyapatite nanoparticles
H ₂ O ₂	Hydrogen Peroxide
PDDA	Poly(diallyldimethylammonium)
CV	Cyclic voltammetry
EMF	Electromotive Force
QCM	Quartz Crystal Microbalance
ISE	Ion-Selective Electrode
MHCF	Metal Hexacyanoferrates
PW	Prussian White
PG/BG	Prussian Green or Berlin Green
PY/PX	Prussian Yellow or Prussian Brown
WE	Working electrode
RE	Reference electrode
CE	Counter/Auxiliary electrode
2H-GE	2H graphite electrode

CHAPTER 1

PURPOSE AND SIGNIFICANCE OF THIS STUDY

1.1 INTRODUCTION

Hydrogen peroxide (H_2O_2) is a simple inorganic compound and its determination plays an important role in various areas such as medicine, biology, environmental, mining, textile and food processes. H_2O_2 is also involved in several biological events and intracellular pathways and is the by-product of enzymatic processes such as those involving, for example, glucose oxidase, cholesterol oxidase and alcohol oxidase¹. H_2O_2 is also a substrate for the enzyme horseradish peroxidase².

On the other hand, CNTs have received a great attention on research in recent years due their high surface areas, their excellent electrical, mechanical and electrochemical properties, therefore the modification of this biosensors with CNTs create a new generation of ultrafast and ultrasensitive biosensors³. The modification of the walls of CNTs with different nanoparticles on biosensors also provide a faster electron transfer rate and catalytic activity towards many biomolecules⁴. Some modified biosensor strongly improve their behavior to immobilize enzymes⁵. Hydroxyapatite (HAp) has a high capacity of adsorption of biomolecules, and also possess exceptional biocompatibility and bioactivity properties⁶. Therefore, the combination of CNTs doped with hydroxyapatite nanoparticles can offer a synergistic effect as biosensors.

Considering the foregoing, this work deals with the development of a new electrochemical sensor with a nanostructured system based on multiwalled carbon nanotubes (MWCNTs) doped with hydroxyapatite nanoparticles for the detection of hydrogen peroxide. The electrochemical sensor measured an electrochemical response when a inorganic electrocatalytic transducer (Prussian Blue) was adsorbed directly onto the surface of modified electrode by Hap-MWCNTs. Prussian Blue (PB) will be used as an electrocatalyst towards hydrogen peroxide reduction.^{7,8}

1.2 GENERAL OBJECTIVE

The main objective of this work, is the development of a new electrochemical sensor that is simple, economic, reliable and highly sensitive to determine hydrogen peroxide, based on multiwalled carbon nanotubes doped with hydroxyapatite nanoparticles and Prussian Blue.

1.2.1 SPECIFIC OBJECTIVES

- Manufacture a graphite electrode based on pencil graphite leads.
- Modify the surface of graphite electrode with MWCNTs and Hap-MWCNTs.
- Characterize the electrochemical behavior of bare and modified graphite electrodes by cyclic voltammetry technique.
- Incorporate and stabilized electrochemically an inorganic electrocatalytic transducer (Prussian Blue) on modified graphite electrodes by cyclic voltammetry and chronoamperometry
- Evaluate and quantify the electrochemical response of the modified electrodes with Prussian blue in hydrogen peroxide solutions.

CHAPTER 2

LITERATURE REVIEW

2.1 SENSORS

The International Union of Pure and Applied Chemistry (IUPAC) defines a chemical sensor as “that device that transforms chemical information into a useful analytical signal”⁹. A chemical sensor is comprised by two components packaged together, with a direct spatial contact, in the same unit, which are: a receptor and a transducer (see Figure 1).

A *receptor* or sensing element receives the physical/chemical stimulus and transforms this information in the form of electrical energy. The sensing element may be composed for materials with distinct molecular units called recognition receptors and also by materials with not distinct recognition sites, but able to interact with the analyte under study¹⁰. A *transducer* is a device capable of transforming the electrical energy of the receptor (an input signal) into a readable, quantifiable and capable of being detected signal (valuable analytical signal) which can further be analyzed and presented in an electronic form¹¹. The analytical signal is transported to an information capture and processing device, for its analysis. It is worth mentioning that a transducer as such does not show selectivity. The transducer part of a sensor is also called a detector, sensor or electrode. The main requirements of a good sensor are high sensitivity, fast response, low cost, and high reliability.

A sensor that incorporates a receptor of biological origin (i.e. enzymes, antibodies, nucleic acids, cells, tissues, and microorganism), connected or integrated within a transducer is called *Biosensor*⁹. Thus, biological receptor system through biochemical mechanisms, allows the detection of biological molecules, whose output signal corresponds to the presence of a certain biomolecule, as well its concentration in the sample. The biological recognition system provides a sensor with a high degree of selectivity for the analyte.

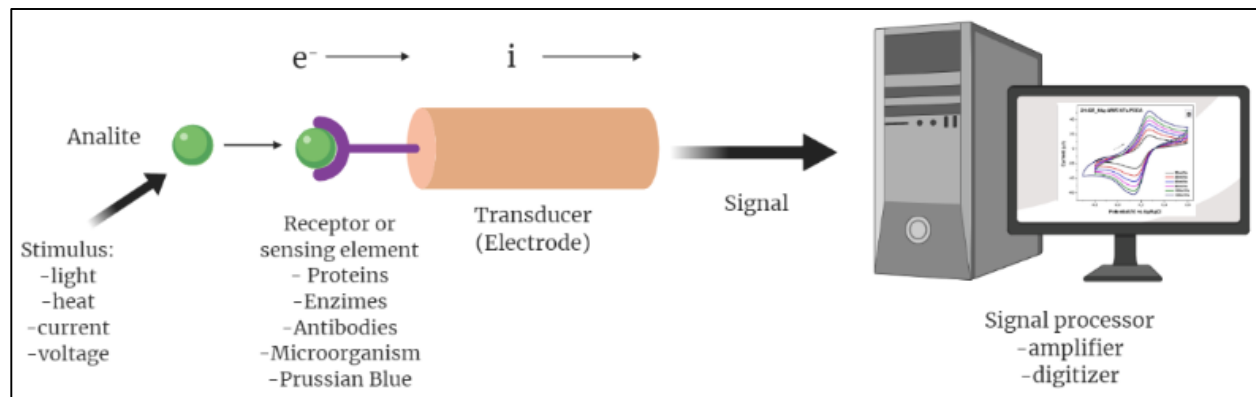


Figure 1. Diagram representing an electrochemical sensor.

2.1.1 CLASSIFICATION OF SENSORS

Since no hard line has been drawn by IUPAC regarding the classification of sensors, there are a few direct approaches that have been associated with the essence of classification such as, mode of reception, field of application, particular given analyte that is detected, measuring method¹¹. According to criteria of detection or measurement mode (electrochemical transduction or detection) sensor are generally divided into three main types, namely: 1) mass-based sensor; 2) optical-based sensor; and 3) electrochemical sensors. For the purpose of this investigation only the electrochemical sensors are described in detail.

2.1.1.1 OPTIC SENSOR

A device whose signal is the result of changes caused by optical interaction between the analyte and receptor¹². For example, a fiber-optic sensors use the reflective properties of light to sense numerous analytes simultaneously. This type of sensors show a high specificity, practicality, and cost effectiveness, as a disadvantage the reagents have a short lifespan under incident light and slow response time as a result of the diffusion of analytes¹³.

2.1.1.2 MASS-BASED SENSOR

The working principle of device consist into transform the mass change at a specially modified surface into a change of a property of the support material¹². The accumulation of the analyte produce the mass change. Piezoelectric sensors are an example, produce an electrical signal when a mechanical force is applied, as it is in the case of Quartz Crystal Microbalance (QCM) model¹⁴.

2.1.1.3 ELECTROCHEMICAL SENSOR

Electrochemical devices measure the response of a system to the electrical potential or current signal. In this sense this sensors and among them biosensors provide high specificity rapid analysis at reasonable costs¹³. Four types of electrochemical sensors exist: 1) potentiometry-based sensors; 2) voltammetry-based sensors; 3) conductometric/capacitive sensor, and 4) impedimetric sensors. For the purposes of this investigation, only the first two types of electrochemical sensors are described.

2.1.1.3.1 POTENTIOMETRY-BASED SENSORS

The potentiometric sensors, measure the potential difference between an indicator electrode (ion-selective electrode, redox electrode, meta/metal oxide electrode) and a reference electrode¹². Thus, the current path between the two electrodes can be highly resistive. An ion-selective electrode (ISE), is an electrochemical sensor based on thin films or selective membranes as recognition elements. Detection limits of the order of 100 nanomoles per litre until 10 picomolar of the total concentration of the ion present in a particular oxidation state⁹. The most common potentiometric devices are pH electrodes.

2.1.1.3.2 VOLTAMMETRY-BASED SENSORS

The voltammetric sensors, including amperometric devices, are based on measurement of the current resulting from the electrochemical oxidation or reduction of an electroactive species,

as a function of applied potential⁹. The resulting current is directly proportional to the bulk concentration of the electroactive species under study. Very low detection limits of down to the picomolar level can be reached¹⁵. These sensors can include chemically inert electrodes, chemically active electrodes, modified electrodes, and sensors with and without (galvanic sensors) external current source are included¹².

The biosensors* are not presented as a special class because the process on which they are based is, in general, common to chemical sensors. They may also be classified according to the biological elements used in the receptor, such as, organisms, tissues, cells, organelles, membranes, enzymes, antibodies, and so on^{12,14}, as shown in Figure 2.

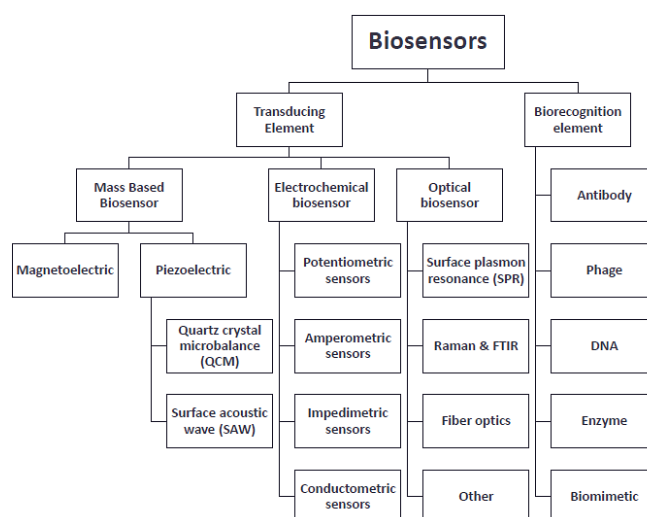


Figure 2. Classification of biosensors based on the transducer element and bio-recognition element.

Taken from reference¹⁴.

* Observation: The present classification of chemical sensors represents one of the possible alternatives, since it can also be classified according to the application to detect, examples are sensors for pH, for metal ions or for determining oxygen or other gases.

2.2 CARBON NANOTUBES

Carbon is one of the most abundant elements in nature and one of the most inquired in Nanotechnology. The Nanotechnology is the manipulation of matter on a nanometric scale (having dimensions of roughly 1-100nm), as example, carbon nanotubes (CNTs) are the results of the application of this technology. Carbon nanotubes are one of the allotropic forms of carbon, together with graphite, amorphous carbon, hexagonal diamond and fullerenes, each one has different and unique properties. Carbon nanotubes are the nanomaterial most investigated by its unique physical, chemical, mechanical and thermal properties¹⁶.

The structure of carbon nanotubes is related to the structure of graphene that is a sheet two-dimensional hexagonal allotrope (graphene is an individual graphite layer). Conceptually, carbon nanotubes are viewed as “rolled-up” structures, therefore, it can be considered as a sheet of graphene rolled into a cylinder.

Carbon nanotubes are built from sp^2 carbon-carbon bond, each atom joined to three neighbors, as in graphite, thus is stronger than sp^3 bonds provides the unique strength. Additionally, presents a seamless structure with hexagonal honeycomb lattices (hexagonal rings) of approximately 1nm diameter and 1 to 100 microns of length^{17,18}. CNTs can have one layer or multiple layers and usually can have a caps at the ends making look like pills.

Multiwalled carbon nanotubes are formed by multiple layers of graphene cylinders (concentric tubes, approximately 50)¹⁹, were the first to be discovered by Iijima on 1991. The graphene cylinders are ordered around a common central hollow, creating layers and depending of those, the inner diameter of MWCNTs can varies between 0.4 nm until a few nanometers, and outer diameter can change from 10-50nm²⁰

Single walled nanotubes. The second type is called single-walled carbon nanotubes (SWCNTs) have only one single layer of graphene cylinders, and possess good uniformity in diameter (1-2 nm), SWCNTs commonly form bundles, and present three different geometries,

such as, armchair, chiral, and Zigzag²¹. Depending of way the graphene is wrapped into a cylinder create a direct effect on the electrical properties of nanotubes.

Carbon nanotubes have some limitations, such poor solubility in water due to their, chemical inertness, difficulty to maintain high quality and minimal impurities, fortunately, there is a solution to overcome this problems, which consist on the modification of the surface of CNTs, that is, functionalization. Various approaches exist for the functionalization of CNTs, and they can be grouped as physical (noncovalent) and chemical (covalent) modifications.

Noncovalent functionalization involves the adsorption of small molecules such the small aromatic compounds, surfactants, biomolecules, and polymers around the wall of CNTs²². This functionalization is generally less perturbative to the intrinsic properties of CNTs, because the adsorption of functional molecules doesn't destroy the conjugated system of the CNTs sidewalls (does not occur the rehybridization ($sp^2 \rightarrow sp^3$), but via van der Waals-type or electrostatic interactions and therefore it does not affect the final structural properties of the material²². It is an attractive alternative method to improve the solubility and processability without not compromise their physical properties. However, the main drawback of this functionalization correspond to the adsorbed molecules, have limited stability and can display changes in their configuration around the CNT, as consequence, the CNTs can reaggregation due to the inherently weak interactions²⁰.

Covalent functionalization use chemical reaction to anchor a strong and stable chemical groups to the end caps of nanotubes or at their sidewalls which have many defects, providing a long-term stability to the dispersion and gives a wide range of possibilities of functionalization with several types of biomolecules^{22,23}. This chemical functionalization change the p-conjugated system of the CNTs sidewalls (occur la rehybridization), as a consequence, altering the intrinsic properties of the CNTs, such as electrical conductivity and mechanical strength, since it destroys the regular graphene-type structure²⁰. Usually, concentrated acids or strong oxidants are often used for CNT functionalization²².

Carbon nanotubes, since their discovery have been utilized in many applications and this is due to their properties, that depend on atomic arrangement (how they are rolled), the diameter and length, morphology, impurities or defects in the walls of the CNTs^{18,22}. Carbon nanotubes are considered the strongest and most flexible molecular material and this is due to its sp² covalent bond and its hexagonal network structure¹⁶. The important and relevant properties of CNT can be appreciated in Table 1.

Table 1. Theoretical and experimentally measured properties of carbon nanotubes.

Property	Carbon nanotubes	Graphite
Lattice structure	(Cylindrical) hexagonal lattice helicity Nanotubes: ropes, tubes arranged in triangular lattice with lattice parameters of $a = 1.7 \text{ nm}$, tube-tube <i>distance</i> = 0.314	Planar hexagonal, plane-to-plane distance $c = 0.335$
Specific gravity	0.8-1.8 gcc ⁻¹ (theoretical)	2.26 gcc ⁻¹
Elastic modulus	~1 TPa for SWNT ~0.3-1 TPa for MWNT	1 TPa (in-plane)
Strength	50-500 GPa for SWNT 10-50 GPa for MWNT	
Resistivity	~5-50 micro-ohm·cm	50 (in-plane)
Thermal conductivity	3000 W m ⁻¹ K ⁻¹ (theoretical)	3000 Wm ⁻¹ K ⁻¹ (in-plane) 6 Wm ⁻¹ K ⁻¹ (c axis)
Thermal expansion	Negligible (theoretical)	-1 × 10 ⁻⁶ K ⁻¹ (in-plane) 29 × 10 ⁻⁶ K ⁻¹ (c axis)
Oxidation in air	>700° C	450-650° C

Taken from reference²².

Since the discovery of carbon nanotubes, have generated enormous interest on the develop biosensor able to detecting biomolecules in areas of health, environment and food¹⁸, due to their properties, such as, surface area, mechanical strength, excellent electrical conductivity and good chemical stability. Biosensors are analytical devices that comprise a) bio-receptor that specifically bind to the analyte, where through a biochemical mechanism gives rise to signal picked up by c) the transducer element; as a typical recognition elements can be enzymes, nucleic acids, antibodies, whole cells, and receptors. The enzymatic biosensors are most developed, being glucose oxidase (GOx)²⁴⁻²⁶ and horseradish peroxidase (HRP)^{2,27-29} the most popular biosensors,

which are based on the use of CNTs to immobilize enzymes. The use of CNTs offer the possibility of develop a biosensors with highly selectivity, sensitivity, and low cost.

One of the major issues when working with enzymes is their stability, because they are very sensitive to their environment, therefore, the modification of the walls of the CNTs with different nanoparticles such as polymers, colloidal gold, and nanosheets³⁰, etc. Recently, there are some interesting researches on integrating nanoparticles, such as, Prussian blue³¹ and hydroxyapatite²⁹, to obtain a synergistic effects as biosensors. For example, hydroxyapatite (HAp) has a high adsorption capacity of biomolecules, in addition to its excellent biocompatibility,^{6,28,29} therefore, the combination of CNTs coated with this nanoparticles has the advantage, apart from improving the biocompatibility, of taking advantage of the properties of the hydroxyapatite.

2.2.1 HYDROXYAPATITE

Hydroxyapatite [HAp, $\text{Ca}_{10}(\text{PO}_4)_6(\text{OH})_2$], is an inorganic compound, member of calcium phosphate family. It possess an equivalent chemical composition and crystal structure to the apatite mineral component of bones and teeth of human body.³² Due its excellent capacity to couple with living bone tissues is consider as a material bioactive, and is used in several biomedical applications, as orthopaedics and orthodontics.³³ HAp has a high adsorption capacity, which its nanoparticles are useful to separate proteins, carrier drug, immobilize enzymes, due their high affinity to biomolecules. In this sense, HAp can be used for develop of hydrogen peroxide,²⁹ glucose,³² phosphate sensors.³⁴

Chemical and physical properties of HAp depend on their crystallinity and its geometrical structure is important for the biomolecules adsorption by electrostatic attractions.³⁵ Hydroxyapatite is an "apatite" mineral with a general formula $\text{M}_{10}(\text{AO}_4)_6\text{B}_2$, where M is calcium (Ca^{2+}), A is phosphorous (P^{5+}) and B is the hydroxyl radical (OH^-), being Ca^{2+} and PO_4^{3-} responsible for the adsorption on its surfaces.^{33,35} Hydroxyapatite is a stoichiometric compound which its atomic radio Ca/P is 1.67, with 39% by weight of Ca, 18.5% P and 3.38% of OH.^{33,36}

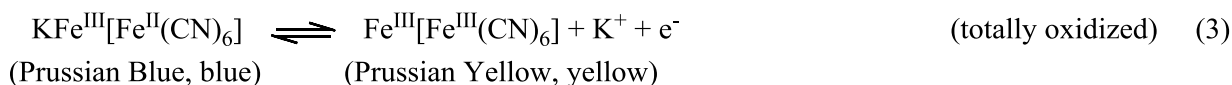
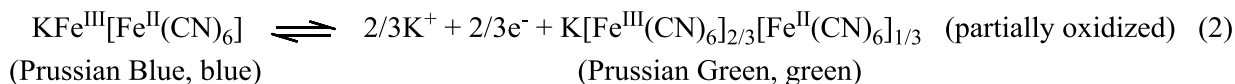
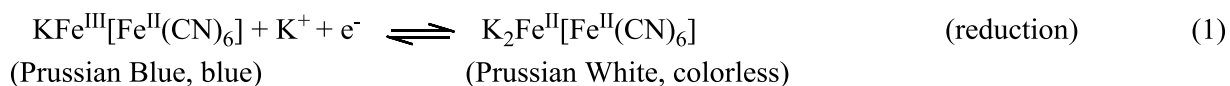
HAp crystallizes in a hexagonal system with a $P6_3/m$ space group, characterized by a sixfold c-axis perpendicular to three equivalent a-axes at 120° angles to each other, where calcium cations (Ca^{2+}) sites surrounded by negatively charged tetrahedral (PO_4^{3-}) units and (OH^-) ions occupy columns parallel to the hexagonal axis, where the phosphate groups network which provides the skeletal framework and gives the structure its stability.^{36,37} According to this, HAp nanoparticles can combine with CNTs are developed in order to enhance the physico-chemical and mechanical properties of hydroxyapatite, creating beneficial synergy effects of these two individual materials, useful to develop biosensors.

2.3 PRUSSIAN BLUE

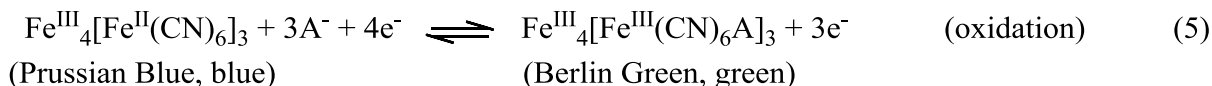
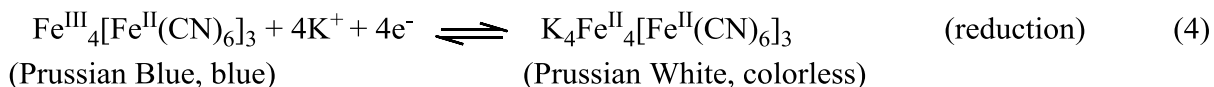
Recent investigations are oriented to use of metal hexacyanoferrates, because present unique properties, such as the capacity to form solid films, and presence of multi-redox centers, usefully to fabrication of sensors. Metal hexacyanoferrates (MHCF) are a mixed-valence compounds, with a general formula $A_x M_y^a [Fe(CN)_6]_z \cdot H_2O$, with A the counteranion, typically an alkaline metal; M^a transition metal and x,y,z stoichiometric numbers, being Prussian Blue is the archetype of these compounds.³⁸ Prussian Blue (PB, or ferric hexacyanoferrate) is the most ancient coordinated compound, that contain a hydrated iron(III) hexacyanoferrate (II) anion, $\{Fe^{III}[Fe^{II}(CN)_6] \cdot mH_2O\}^-$, with $m = 14-16$, and various cations, such as K^+ , NH_4^+ or Na^+ .³⁹ Prussian Blue has been received great importance, due their electrochromic⁴⁰ and electrocatalytic⁴¹ properties crucial for the development of chemical and biological sensors. PB is considered as an electrochemical mediator or transducer which is used as component of H_2O_2 (bio)sensors due to its high electrocatalytic activity toward H_2O_2 reduction at relatively low-potential.^{42,43} PB is characterized for its deep blue colour, and this due to the mixed-valence of iron ions that contains, originating an electronic transition from the Fe^{II} to Fe^{III} ion⁴⁴ caused by absorption of the orange-red light of visible spectrum at 700nm.^{39,45}

2.3.1 ELECTROCHEMISTRY PROPERTIES OF PRUSSIAN BLUE

As seen before, PB crystals are composed of all possible iron redox state combinations, therefore, they give pass to reduced and oxidized forms, which have been colorfully named: *Prussian White (PW)*, also known as “Everitt’s salt”; *Prussian Blue (PB)*; *Prussian Green (PG)*, also called “Berlin Green”; and *Prussian Yellow (PY)*, also called “Prussian Brown”.^{46,47} The reduction and oxidation reactions of “soluble-PB”, is describe as follows:^{42,48}



Evidently, Prussian Green is the result of mixed of Prussian Blue and Prussian Yellow. Finally, the redox reactions of “insoluble-PB”, are describe as follows:^{42,48}



According to Itaya and co-workers⁴² Prussian White (reduced form of PB), is able of to reduce O_2 and H_2O_2 at a very rapid catalytic rate at low potentials, due their zeolite structure which may allow diffusion of small molecules into the lattices, such O_2 and H_2O_2 (low molecular weight molecules).⁴² Additionally, the oxidized form of PB (Prussian Green or Prussian Yellow) also shows a catalytic activity for the oxidation of H_2O_2 . Due to the electrocatalytic properties of

PB toward the reduction of hydrogen peroxide, Prussian Blue is usually considered an artificial enzyme peroxidase.^{7,49}

2.4 ELECTROCHEMICAL SENSING OF HYDROGEN PEROXIDE

Due the important analytical role plays hydrogen peroxide on biological processes and its application in different industries, leads to the development an efficient, reliable and economical electrochemical H_2O_2 sensors. Nowadays, the determination of hydrogen peroxide there is considerable interest in clinical diagnostic, especially in oxidative stress, because is related with severe pathological conditions such as diabetes, atherosclerosis, renal disease, cancer, aging, and other conditions.⁵⁰ Additionally, various biochemical reactions involving oxidase enzymes (alcohol oxidase, urate oxidase, amino acid oxidase, cholesterol oxidase, glucose oxidase) generate hydrogen peroxide as side product or byproduct.¹

Different techniques there are to hydrogen peroxide determination, such as fluorimetry,⁵¹ chemiluminescence,⁵² and spectrophotometry,⁵³ which are complex, expensive and time consuming. However, electrochemistry can offer simple, rapid, sensitive, and cost effective means since H_2O_2 is an electroactive molecule.¹ As consequence, electrochemical sensors with high sensitivity and low detection limits of detection of H_2O_2 are desirable, and there are several nanomaterials and electrocatalytic compounds used for electrocatalytic hydrogen peroxide sensing, such as Prussian blue (PB),⁵⁴ enzymes,^{28,55} carbon nanotubes (CNTs),³ nanoparticles (Hap),⁶ and transition metals (Ag, Pt, Au, Pd).⁵⁶

CHAPTER 3

EXPERIMENTAL

3.1 TECHNIQUES OF CHARACTERIZATION

3.1.1 CYCLIC VOLTAMMETRY

Cyclic Voltammetry (CV) is one of the most important electrochemical techniques, mainly in the study of redox processes, reaction mechanisms, electrocatalytic properties, etc. CV is characterized for a perturbation of applied potential that increases or decreases linearly with time (linear potential sweep) in triangular form at an electrode (working electrode).

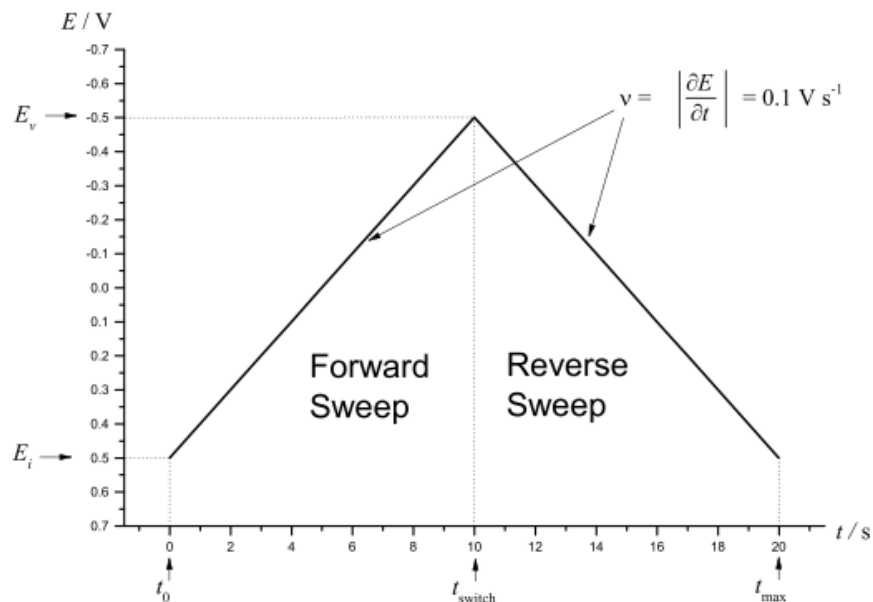


Figure 3. The waveform of the potential applied during a typical cyclic voltammetry experiment. The initial potential (E_i) is 0.5V, the vertex potential (E_v) is -0.5V, and the scan rate (v) is 0.1 V s^{-1} . Taken from reference⁵⁷.

According to Figure 3, it can be seen a vertex potential (E_v), which is the upper limit of potential and the slope of the sides is the scan rate (dE/dt). The response to the perturbation is a measure of current (i) as a function of the applied potential (E). A plot of the current against applied potential is called a voltammogram, as shown in Figure 4. The magnitude of this current is proportional to the concentration of the analyte in the solution, which allows cyclic voltammetry to be used in an analytical determination of concentration.⁵⁸

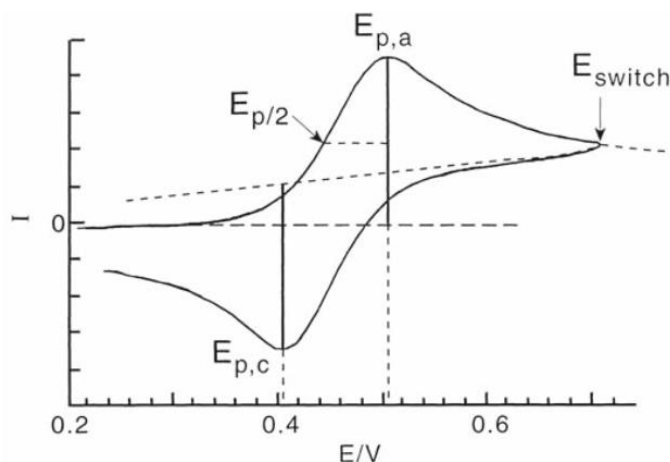


Figure 4. A typical cyclic voltammogram produced by the application of the potential waveform. Taken from reference⁵⁹

3.1.1.2 CHARACTERISTIC PARAMETERS OF A CYCLIC VOLTAMMOGRAM

In a cyclic voltammogram is common that exist several peaks, and the magnitudes of these are important parameters which are associated with redox reaction of specie under study. The anodic peak current (i_{pa}), the cathodic peak current (i_{pc}), the anodic peak potential (E_{pa}) and cathodic peak potential (E_{pc}) are shown on the Figure 4.

3.1.1.2.1 REVERSIBLE ELECTRON TRANSFER PROCESS

A redox couple in which both species rapidly exchange electrons with the working electrode is termed an electrochemically reversible couple. For reversible electrochemical reaction the cyclic voltammogram recorded at 25°C has a certain well defined characteristics:

- 1 The half-wave potential ($E_{1/2}$) for a reversible couple is centered between E_{pa} and E_{pc} .

$$\Delta E_{1/2} = \frac{E_{pa} + E_{pc}}{2} \quad (6)$$

- 2 The number of electrons transferred in the electrode reaction (n) for a reversible couple can be determined from the separation between the peak potentials.

$$\Delta E_p = E_{pa} - E_{pc} \cong \frac{0.059}{n} mV \quad (7)$$

- 3 The peak current for a reversible system is described by the Randles-Sevcik equation for the forward sweep of the first cycle.

$$i_p = 0.4463 \left(\frac{F^3}{RT} \right)^{1/2} A n^{3/2} D^{1/2} C_o \nu^{1/2} \quad (8)$$

where i_p is peak current, n is electron stoichiometry, A is electrode area (cm^2), D is diffusion coefficient (cm^2/s), C_o is concentration (mol/cm^3), ν is scan rate (V/s), F is Faraday constant ($96485 \text{ C}/\text{mol}$), R is the universal gas constant ($8.314 \text{ J mol}^{-1} \text{ K}^{-1}$), and T is the absolute temperature (298 K). Accordingly, i_p increases with $\nu^{1/2}$ and is directly proportional to concentration ($i_p \propto \sqrt{\nu}$).

- 4 The values of i_{pa} and i_{pc} should be identical for a simple reversible (fast) couple.

$$\frac{i_{pa}}{i_{pc}} = 1 \quad (9)$$

3.1.2 CHRONOAMPEROMETRY

Chronoamperometry (CA) is an electrochemical technique that studies the kinetics of chemical reactions, controlled diffusion processes and adsorption. This technique is characterized by applying an initial potential (E_1) in which a non-Faraday reaction occurs, followed of a stepping potential (E_2) in which the electrochemical reactions of interest take place. This last potential can be of reduction or oxidation. Is common that the solution not stirred. The resulting current is observed as a function of time, as shown in Figure 5. Chronoamperometry is related to the Cottrell equation (11), which describes the change in current with respect to time in a controlled potential experiment.

$$i(t) = n F A C_o \sqrt{\frac{D}{\pi t}} \quad (10)$$

In the Cottrell equation, the current (i) is dependent of F (Faraday's constant), n the number of transferred electrons per molecules, A the electrode area, C_o the analyte concentration, D the diffusion coefficient and time t . From the Cottrell equation the current depends on the rate at which the analyte diffuses to the electrode.⁶⁰

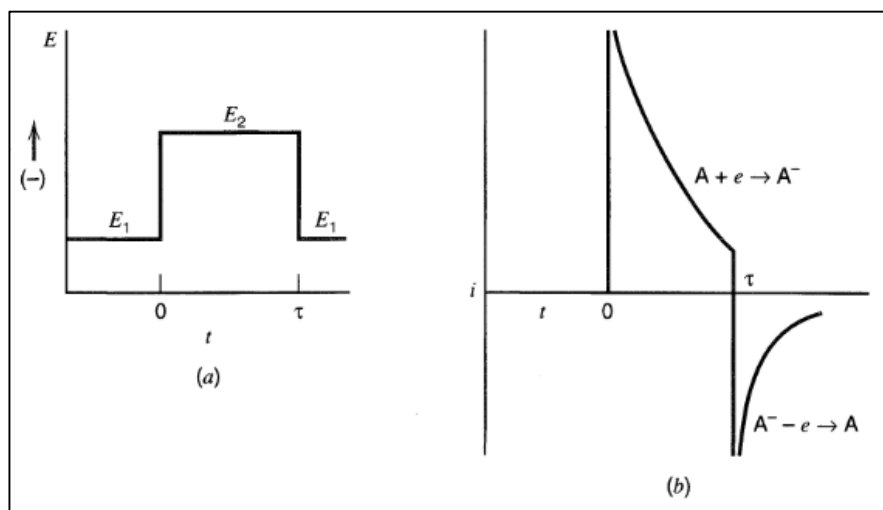


Figure 5. Double potential step chronoamperometry. (a) Typical waveform. (b) Current response. Taken from reference⁶⁰.

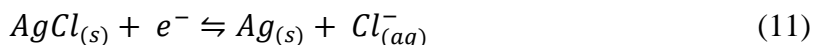
3.2 ELECTRODES AND ELECTROCHEMICAL CELL

3.2.1 WORKING ELECTRODE (WE)

The working electrode is the electrode in which the electrochemical event of interest occurring. Usually, inert material such metal, semiconductor, graphite or conducting polymers are component of the electrode. Generally, are fashioned into disks surrounded by a chemically inert should be made from Teflon, glass, or epoxy. The size and shape of the electrode surface influence on the voltammetric response. Since the event of interest occurs at the surface, this requires that the surface of the electrode be extremely clean and its area well defined. The common procedure of polishing is based on the use of water-alumina slurry of different particle sizes (0.03-1.0 μm), with figure- eight motions on a cloth polishing pad. To remove particles, the electrode is sonicated with distilled water.⁶¹

3.2.2 REFERENCE ELECTRODE (RE)

Reference electrode is an electrode which has a well-defined and stable equilibrium potential and is used a reference point against the potential of other electrodes can be measured in an electrochemical cell.⁶¹ The most common reference electrodes used in aqueous media are saturated calomel electrode (SCE), standard hydrogen electrode (SHE) and the Ag/AgCl electrode. The latter is the most used and is composed of a silver wire contained in a KCl saturated solution. The half-reaction for this reference electrode is as follows:



3.2.3 COUNTER ELECTRODE (CE)

The counter electrode is also known as auxiliary electrode, whose purpose is close the current circuit in the electrochemical cell.⁶¹ Usually, is made of inert material (Pt, Au, graphite) and does not participate of electrochemical reaction. Because the current is flowing between the

WE and the CE, the total surface area of the CE (source/sink of electrons) must be higher than the area of the WE so that it will not be a limiting factor in the kinetics of electrochemical process under investigation⁶².

3.3 REAGENTS AND SOLUTIONS

The experiments were carried out under ambient conditions of temperature and pressure. The MWCNTs and HAp-MWCNTs used for this thesis, they were donated by Gema Gonzalez Ph.D., professor of the school of Physical Science and Nanotechnology at the Yachay Tech University, product of the work done by Yaquelin Sarmiento.⁶³

All chemicals used in this thesis were from commercial sources with an analytical purity and used as received. Iron (III) chloride hexahydrate ($\text{FeCl}_3 \cdot 6\text{H}_2\text{O}$), potassium ferricyanide [$\text{K}_3(\text{Fe}(\text{CN})_6$)], potassium chloride (KCl), sodium hydroxide (NaOH), acid chloride (HCl, 37%), and hydrogen peroxide (H_2O_2 , 30%) were purchased from Sigma-Aldrich, USA. Potassium phosphate monobasic (KH_2PO_4 , 99% of purity) was purchased from Jade Scientific, Canada, and N, N-Dimethylformamide (DMF) was purchased from Fisher Scientific, UK.

PDDA solution: Poly(diallyldimethylammonium chloride) (PDDA, $\text{Mw} < 100.000 \text{ g mol}^{-1}$ in 35wt% aqueous solution) were purchased from Sigma-Aldrich, USA, and its solution was prepared in 0.5 M NaCl at a concentration of 1mg/mL. PDDA is used as an electrostatic stabilizer between the layers of MWCNTs and the surface of graphite electrode

Supporting electrolyte: The electrolyte solution used for every experiment was a phosphate buffer saline (PBS) at a concentration of 0.1 M and pH of 7.4, which was prepared by using 250 mL of 0.1 M KH_2PO_4 and the pH adjusted with 100 mL of 0.2 M NaOH, into a volumetric flask of 500 mL.

Stock solutions of H_2O_2 : Hydrogen peroxide (30%) solution at a concentration of 0.1 M was prepared by dissolving 250 μL in 25 mL of distilled water and stored at 4°C when not in use. The working standard solutions from 1 to 10 mM were freshly prepared before used and purged

with pure nitrogen during 1 min to eliminate de oxygen during the experiments. Distilled water was used for all experiments.

MWCNTs and Hap-MWCNT suspension: All the carbon nanotubes were donated, with a previous characterization and functionalization.⁶³ A 5.0 mg of MWCNTs was dispersed in 1 mL of DMF (polar solvent) by sonication for 30 min, and then is stored in a dark place at room temperature for further study. The same procedure applies to HAp-MWCNTs, but with a sonication of 10 min.

3.4 INSTRUMENTATION

Cyclic Voltammetry (CV) and Chronoamperometry (CA) experiments were performed with two Autolab potentiostats-galvanostats models PGSTAT302N and PGSTAT204 (Metrohm, Utrecht, Netherlands) with NOVA 2.1 software for system controlling and data acquisition.

A platinum (Pt) wire as a counter electrode (CE) and a commercial Ag/AgCl (Sat KCl, CH Instruments) as a reference electrode (RE) was used. The working electrode (WE) was a graphite electrode fabricated using 2H-pencil graphite leads. The home-made electrochemical cell with three electrode arrangement shown in Figure 6, was used for all electrochemical experiments

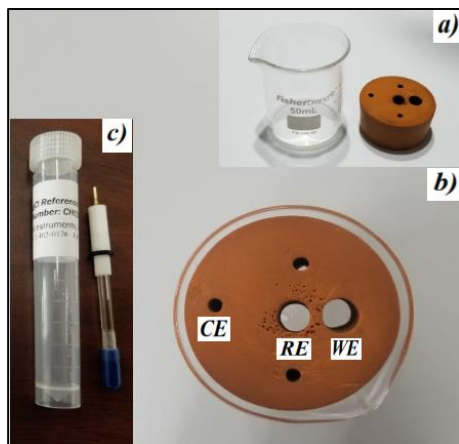


Figure 6. Design of electrochemical cell. a) Beaker and rubber stopper, b) Holes for electrochemical electrodes (CE, RE, WE) and c) commercial Ag/AgCl (Sat KCl, CH Instruments) reference electrode.

Abbreviations: CE=Counter Electrode, RE= Reference Electrode, WE= Working Electrode.

3.5 GRAPHITE ELECTRODE MANUFACTURE

A tubing glass of 7 mm of inner diameter and 6.5 cm of length, as a source of graphite a commercial 2H-pencil graphite (Staedtler, Germany) was used, and a commercial epoxy resin were materials used to assembly of electrode. At first, the 2H graphite leads was obtained removing carefully the outer wooden sheath, then was cutted until obtain a length of 8 cm. As next step, the 2H graphite lead was cleaned in an ultrasonic bath of acetone/water during 10 min. Finally, the 2H graphite lead was dried at room temperature and placing into the center of the tubing glass, then was sealed the edges between glass and graphite lead with epoxy resin. For the resin to exert a good compaction, it was left to dry for 24 hours at room temperature. The excess of epoxy resin into the edge of electrode was removed by using a sharp blade and the surface of electrode was smoothened through mechanical polishing with using emery paper #500, #1200, #2500, followed of a polishing with alumina suspension of different grain size (1.0 μm and 0.05 μm) into a cloth polishing pad during 2 minutes and rinsed with distilled water.⁶¹ To remove any particles of the surface of electrode, required a sonication treatment during 5 minutes in an

acetone/water solution (1:1). As a result, a 2H graphite electrode (GE) with a diameter (\varnothing) of 2 mm is obtained, ready to be subjected to electrochemical tests, as illustrate Figure 7.

The parameter of pencil graphite leads selection, was according to Gong and co-workers⁶⁴, they showed that harder (2H) composite pencil graphite electrodes (CPGE) provides of excellent reversibility for a redox system, which is essential for qualitative and quantitate analysis. The pencil graphite leads is a composite which contain graphite, clay and a binder (wax, resins). The use of letters are common to classify the pencil: H-group (hardness) and B-group (blackness or softness), while the numbers indicated the diameter size of the pencil lead. Additionally, the B-group contains more graphite than H-group, whereas HB-type pencil leads has equal proportion of graphite and clay.⁶⁵



Figure 7. Construction of 2H-graphite electrode. a) Commercial 2H-pencil graphite (Staedtler, Germany), b) Glass tubing, and c) Epoxy resin.

Prior to use, the 2H graphite electrode surface was previously mechanical polished with an emery paper #A99-240, to activate the surface of electrode through creation of defects⁶⁶. Afterwards, was again polished with 1.0 μm alumina slurry, and sonicated during 5 min in a distilled water to remove any residual particle. Finally, the electrode was dried at 50°C in an oven during 5 min and cooled at room temperature, now the electrode is ready to be modified.

3.6 PREPARATION AND CHARACTERIZATION OF MODIFIED ELECTRODES

Onto the surface of the 2H graphite electrode, previously treated, 10 μL of the suspension of MWCNTs or HAp-MWCNTS is pipetted, and then it is dried in an oven at 50° C for 7 min. Afterwards, 10 μL of the PDDA solution is pipetted on the surface of the modified electrode, and once again proceed to dry at 50° C, but for 10 min. This procedure was based on electrostatic interactions, between the negatively charged of carbon nanotubes and a positively charged polymer layer.⁶⁷

The graphite electrode (bare electrode) and modified electrodes were characterized by cyclic voltammetry (CV) using Autolab potentiostat model PGSTAT302N (Metrohm, Utrecht, Netherlands), at ambient temperature and pressure. The electrochemical measurements were performed to evaluate the current response of the electrodes immersed in a solution of 4 mM $\text{K}_3[\text{Fe}(\text{CN})_6]$ containing in 0.1 M PBS as the supporting electrolyte. The range potential of cyclic voltammetry was set from -0.2 to +0.6 V (versus Ag/AgCl) with scan rates from 20 to 100 mVs^{-1} .

3.7 ELECTRODEPOSITION OF PRUSSIAN BLUE

The electrochemical deposition of Prussian Blue film onto modified graphite electrodes, was according to the procedure described by Karyakin and co-workers.⁷ The deposition of PB was carried out by chronoamperometry through Autolab potentiostat model PGSTAT204 (Metrohm, Utrecht, Netherlands), applying a constant potential of 0.4 V during 60 s, at the solution: 2.5 mM $\text{K}_3[\text{Fe}(\text{CN})_6]$ + 2.5 mM $\text{FeCl}_3 \cdot 6\text{H}_2\text{O}$ containing in a supporting electrolyte of 0.1 M HCl + 0.1 M KCl (pH=2). The PB films deposited were activated cycling the applied potential in a range -0.15 and +0.5 V (versus Ag/AgCl), at scan rate of 50 mVs^{-1} , several times in the same supporting electrolyte solution, until obtain a stable voltammetric response. (see Figure 8 and 9).

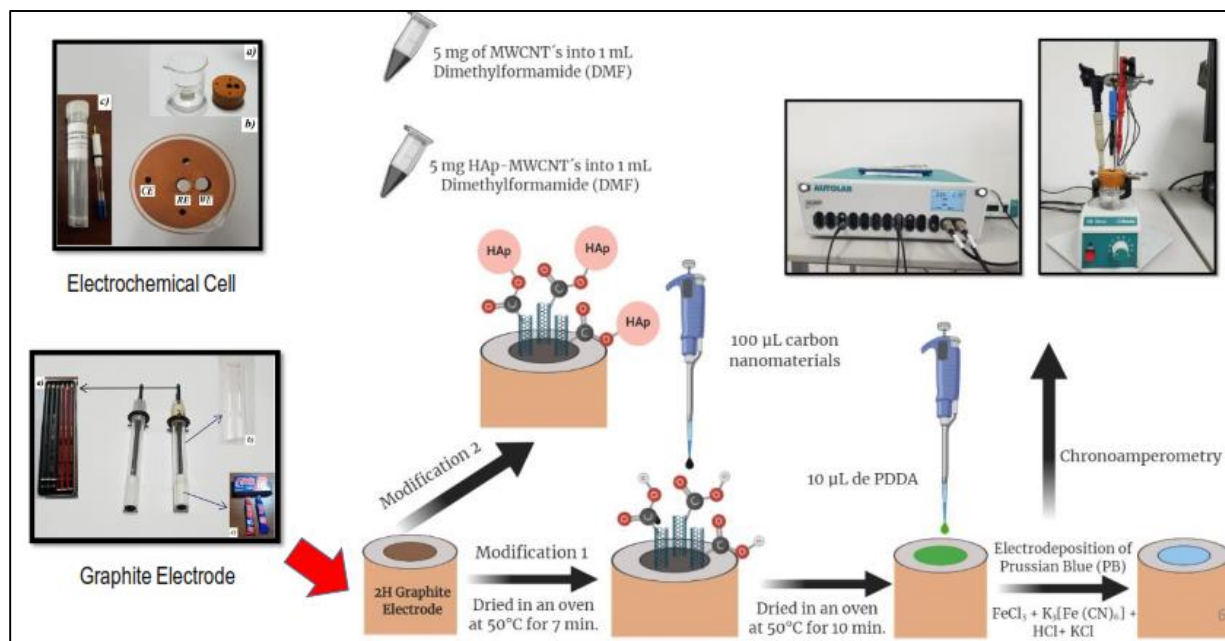


Figure 8. Scheme of experimental procedure

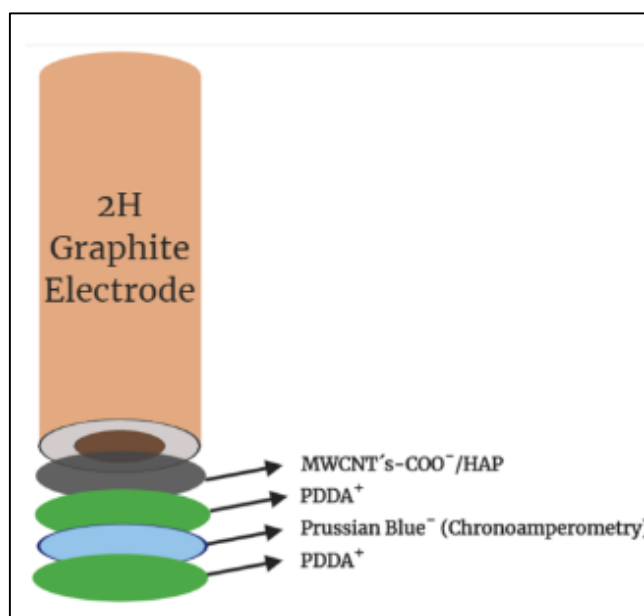


Figure 9. Scheme of assembly of electrochemical sensor.

CHAPTER 4

RESULTS AND DISCUSSION

According to the purpose of this thesis, carbon nanomaterials that were used as a component of the electrochemical sensor for the detection of hydrogen peroxide, were not synthesized as part of this work. However, in this section their characterization is described, thanks to the fact that information was provided. by Gema Gonzalez Ph.D., professor of the school of Physical Science and Nanotechnology at the Yachay Tech University, product of the work done by Yaquelin Sarmiento.⁶³

4.1 CHARACTERIZATION OF CARBON NANOTUBES (CNT)

4.1.1 FOURIER TRANSFORMED INFRARED SPECTROSCOPY (FTIR)

For the purpose of this work the information obtain of CNT_r-B, was relevant, because are the carbon nanomaterials used on the assembly the electrochemical sensor.

The FTIR spectra of the different carbon nanotubes are presented in Figures 10 and 11. Figure 10 shows the spectra of the nanotubes from 400 to 4000 cm^{-1} ; while Figure 11 shows an enlarged section of this region, ranging from 400 to 1800 cm^{-1} . The FTIR spectra of the carbon nanotubes are similar to the target with which the tablet was prepared (KBr). In figures 11 no signals of the functional groups frequently found in oxidized CNTs are observed, such as carboxylic groups ($\approx 1740 \text{ cm}^{-1}$), hydroxyls ($\approx 3500 \text{ cm}^{-1}$) and esters ($\approx 1100 \text{ cm}^{-1}$); This may be due to the small number of functional groups found in the walls of these nanotubes. The functional group $\text{C} = \text{C}$ (≈ 1550 and 1200 cm^{-1}), which is inherent in carbon nanotubes, is also not detected in these figures. However, small bands between 400 and 600 cm^{-1} are identified in Figure 11, which characterize this type of CNT (fingerprint region). In addition, small bands between 1000 and 1200 cm^{-1} are observed mainly in the FTIR spectrum of functionalized CNTs, which are due to vibrations of the C-H and C-O-C bonds.

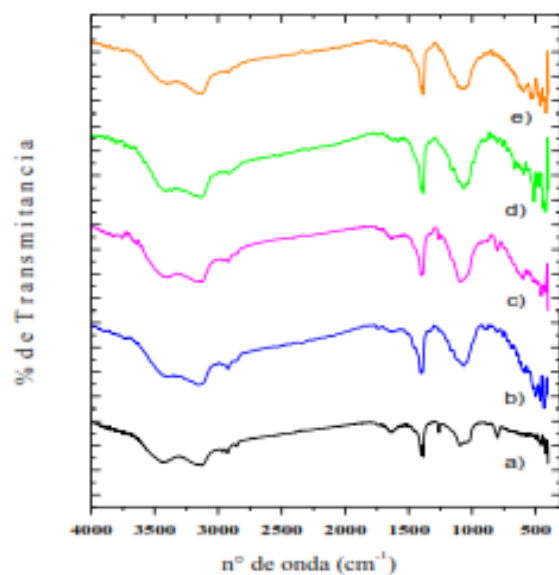


Figure 10. FTIR spectrums of CNTs of 400 to 4000cm⁻¹: a) KBr (Blank), b) CNT pristine, c) CNT_p, d) CNT_r-B, and e) CNT_r-A.

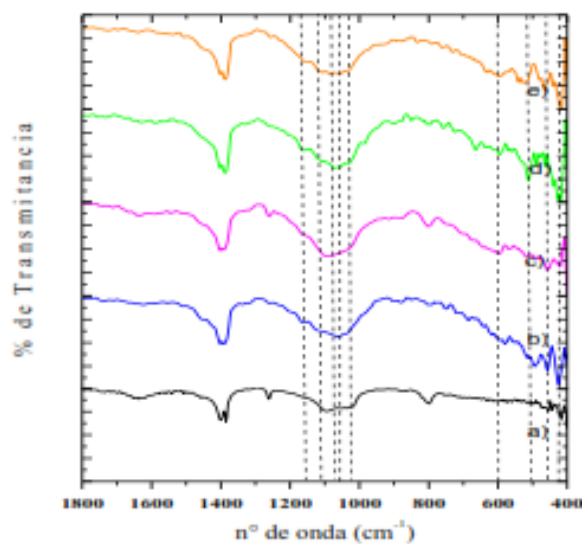


Figure 11. FTIR spectrums of CNTs of 400 to 1800cm⁻¹: a) KBr(Blank), b)CNT pristine, c) CNT_p, d) CNT_r-B, and e) CNT_r-A.

4.1.2 X-RAY DIFFRACTION (XRD)

From Figure 12, two characteristic reflections of the graphene 002 and 100 planes in carbon nanotubes can be observed. These reflections are approximately 25° and 43° , respectively. The angle of diffraction of the plane (002) decreases and the interplanar distance of the NTC increases with respect to that of graphite, which is due to the curvature and different orientation of the graphene sheets with respect to the axis of the nanotube. Note in Figure 12 that the patterns of the different carbon nanotubes do not differ much from each other, which indicates that there are no structural changes in the CNTs in the different steps of the functionalization process. To comparing the diffraction angle and the interplanar distance of the peaks observed in Figure 12 with those reported in JCPDS 75-1621 data for HAp, in Table 2.

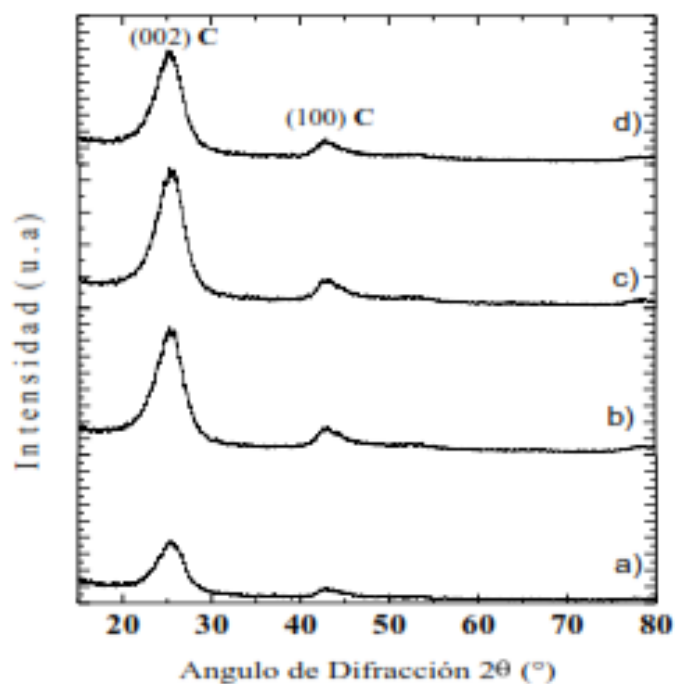


Figure 12. DRX patterns of: a) pristine CNTs, b) CNT_pB, c) CNT_fB and d) CNT_fA.

Table 2. Characteristic DRX data of hexagonal graphite.

Diffraction angle (2θ)	Interplanar distance (\AA)	Miller Index
JCPDS	JCPDS	JCPDS
75-1621	75-1621	75-1621
26,228	3,3950	(002)
42,214	2,1390	(100)
44,365	2,0402	(101)
50,381	1,8092	(102)
53,974	1,6975	(004)
59,404	1,5546	(103)
70,804	1,3296	(104)
77,177	1,2350	(110)

Taken from reference ⁶³.

4.1.3 TRANSMISSION ELECTRON MICROSCOPY (TEM)

Figure 13 shows the images of the different CNTs, it can be seen that there are no significant changes in the structures of the CNT obtained in the different steps of the functionalization process, which indicates that there is little destruction of the tube walls, thereby ensuring that functionalized CNTs retain the intrinsic properties of pristine CNTs. To demonstrate this, the distribution and average diameter of the different CNTs were determined from these figures, which are presented in Table 3.

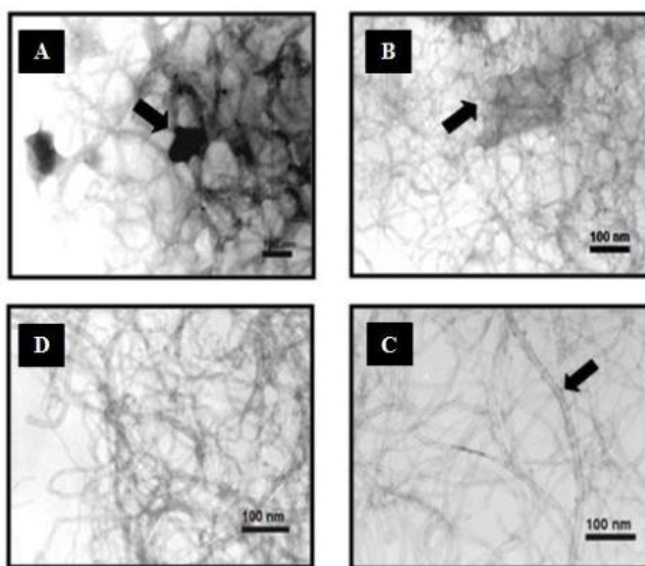


Figure 13. CNT TEM images: a) Pristine CNTs, b) CNT_p, c) CNT_{f-B}, d) CNT_{f-A}.

Table 3. Diameter of the CNT obtained in the different steps of the functionalization process.

CNTs Types	Pristine CNTs	CNTp-B	CNTf-B	CNTf-A
Diameter(nm)	18±4	13±4	12±2	12±3
Distribution of diameter (nm)	12-25	7-21	7-16	6-18

Taken from reference ⁶³.

It is evident when comparing the images that the pristine CNTs present impurities on most of the nanotubes, shown by the arrow in the image A. While in the CNT_f-B and CNT_f-A, a complete disappearance of these impurities is evidenced; however, image D shows that functionalized CNT_f-A do not show complete purification, since metal particles are observed in some nanotubes.

4.2 CHARACTERIZATION OF PURE HYDROXYAPATITE (HAP)

4.2.1 FOURIER TRANSFORMED INFRARED SPECTROSCOPY (FTIR)

The synthesized pure Hydroxyapatite has characteristic infrared bands of this substance $[\text{Ca}_{10}(\text{PO}_4)_6(\text{OH})_2]$, which are shown in Figure 14.

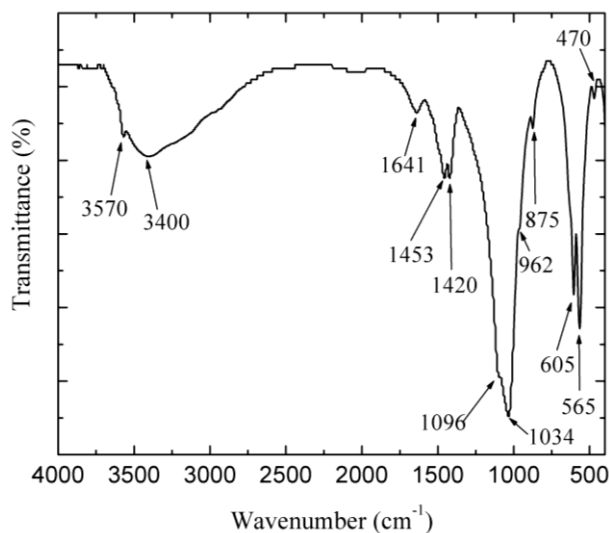


Figure 14. FTIR spectrum of synthesized HAP.

The bands at 470, 565, 605, 962, 1034 and 1096 cm^{-1} correspond to the bonds changes of the PO_4^{3-} groups present in the HAp. In this sense, the band at 470 cm^{-1} corresponds to the bendings ν_2 of the O-P-O bond, the bands at 565 and 605 cm^{-1} to the bendings ν_4 of this same bond, the band at 962 cm^{-1} is due to symmetrical stretching ν_1 of the P-O bond and the bands at 1034 and 1096 cm^{-1} at the asymmetric stretching ν_3 of this same bond. The broad band around 3400 cm^{-1} and the band at 1641 cm^{-1} correspond to vibrations in the molecules of absorbed water. The bands at 1452, 1420 and 875 cm^{-1} correspond to vibrations of CO_3^{2-} and HPO_4^{2-} groups included in the HAp structure at the time of synthesis. The weak band at 3570 cm^{-1} is due to tensions of the OH^- group; while the 630 cm^{-1} band that also corresponds to OH^- group voltages is not observed in the spectrum, which is due to the competition of the CO_3^{2-} and HPO_4^{2-} ions with the OH^- . In addition, the evidence of the band at 3570 cm^{-1} proves that the reaction product is HAp, since the other calcium phosphates do not have this band.

4.2.2 X-RAY DIFFRACTION (XRD)

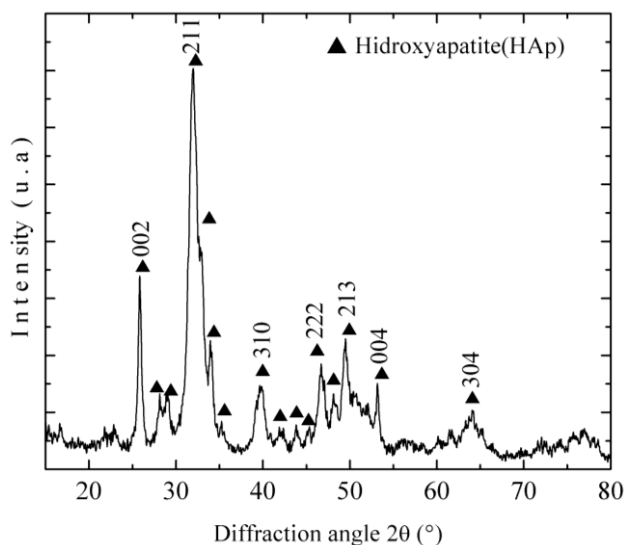


Figure 15. Diffractogram of the synthesized HAp. Taken from reference ⁶³

The Figure 15 shows the diffractogram of the HAp synthesized by the chemical precipitation method. The peaks obtained from the diffractogram of the synthesized HAp

correspond well with those established for the stoichiometric HAp; this is demonstrated by comparing the diffraction angle and the interplanar distance of the peaks observed in Figure 15 with those reported in JCPDS 09-0432 data for HAp, in Table 4.

Table 4. Reflections observed in XRD of stoichiometric hydroxyapatite.

Diffraction angle (2 θ)		Interplanar distance (Å)		Miller Index
Measure	JCPDS 09-0432	Measure	JCPDS 09-0432	JCPDS 09-0432
----	21,82	----	4,070	(200)
----	22,90	----	3,880	(111)
25,84	25,88	3,448	3,440	(002)
28,13	28,13	3,172	3,170	(102)
29,07	29,00	3,071	3,080	(210)
32,00	31,77	2,800	2,814	(211)
----	32,20	----	2,778	(112)
32,99	32,90	2,715	2,720	(300)
33,98	34,05	2,638	2,631	(202)
39,87	39,82	2,269	2,262	(310)
41,92	42,03	----	2,148	(311)
46,69	46,71	1,945	1,943	(222)
48,12	48,10	1,891	1,890	(312)
49,50	49,47	1,841	1,841	(213)
----	50,49	----	1,806	(321)

----	51,28	----	1,780	(410)
----	52,10	----	1,754	(402), (303)
53,15	53,14	1,723	1,722	(004), (411)
----	55,90	----	1,644	(322), (223)
----	61,66	----	1,503	(214), (421)
----	63,01	----	1,474	(502)
64,07	64,08	1,453	1,452	(510)
----	65,03	----	1,433	(511)
----	75,58	----	1,257	(215)
----	77,18	----	1,235	(513)
----	78,23	----	1,221	(522)

Taken from reference ⁶³.

On the other hand, it can be inferred that the HAp obtained is of nanometric size, since the peaks around the planes 211, 213 and 304 overlap, making its definition impossible.

4.2.3 TRANSMISSION ELECTRON MICROSCOPY (TEM)

HAp particles synthesized by the chemical precipitation method are nanometric in size and bar-shaped, as seen in Figure 16; they have a length of 45 to 100 nm and a diameter of approximately 20 nm. In addition, it is observed that HAp particles are agglomerated, which is due to the large surface energy of nano-sized particles, since nanometric-sized particles tend to agglomerate to decrease their large surface energy.

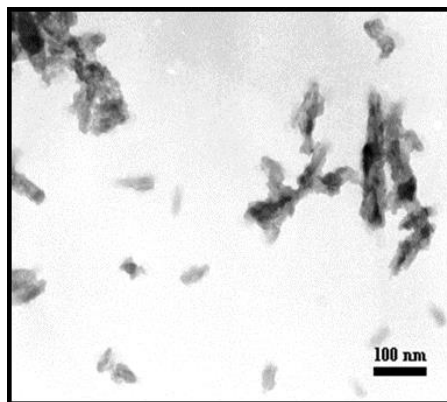


Figure 16. TEM image of the synthesized HAp.

4.3 CHARACTERIZATION OF NANOSTRUCTURED SYSTEMS WITH HYDROXYAPATITE (CNT/HAp)

4.3.1 FOURIER TRANSFORMED INFRARED SPECTROSCOPY (FTIR)

The figure 17 and Table 5 show that the CNTf / HAp nanostructured compounds (36) and CNTf/HAp (100) exhibit the same bands as HAp, with the exception of the band at 3570 cm^{-1} , which represents the OH^- groups of this substance. This result probably indicates the existence of some interaction between the CNTf and the HAp. Also, it is observed that the bands corresponding to HAp are more intense in the CNTf/HAp compound (36) than in the CNTf / HAp compound (100), which shows that there is a greater amount of HAp in this compound, as is be expected. Significant differences of these compounds with respect to HAp can be observed in the right part of Figure 17, where the CNT / HAp compounds have characteristic bands of the CNTf, in the region ranging from 400 to 515 cm^{-1} .

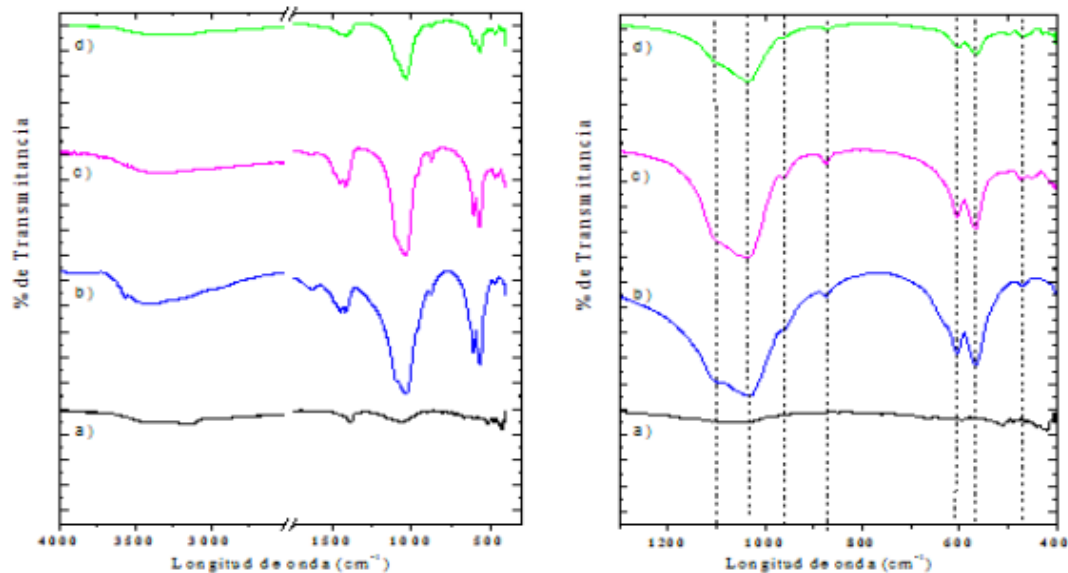


Figure 17. FTIR spectra of CNT_f / HAp nanostructured systems: a) CNT_f.B, b) HAp, c) CNT_f / HAp (36) and d) CNT_f / HAp (100).

Table 5. FTIR bands of the HAp and the CNT_f / HAp (36) and CNT_f / HAp (100) systems.

Compounds	FTIR Bands (cm ⁻¹)									
HAp	3570	1458	1421	1096	1034	958	875	605	566	475
CNTf/HAp(36)	----	1456	1420	1097	1039	957	875	604	567	472
CNTf/HAp(100)	----	1455	1420	----	1036	957	874	604	565	499
										468

Taken from reference ⁶³.

The compounds CNT_f / HAp (36) and CNT_f / HAp (100) have characteristic bands of HAp, as shown in Figure 69, being more intense and defined in the compound CNT_f / HAp (36), which indicates the existence of greater amount of HAp in this compound, as obtained in the FTIR analysis.

4.3.2 X-RAY DIFFRACTION (XRD)

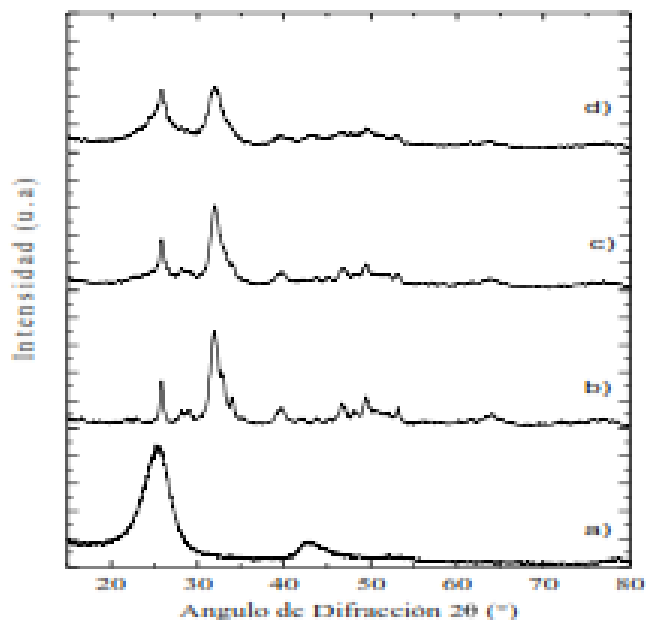


Figure 18. XRD standards of the CNT_f/HAp nanostructured compounds: a) CNT_f-B, b) HAp, c) CNT_f/HAp (36) and d) CNT_f/HAp (100).

The Figure 18 show the DRX patterns of the compounds CNT_f/HAp. In the CNT_f/HAp compound (100) the intensity of the peak of the plane (002) at $2\theta = 25.9^\circ$ increases with respect to that of HAp, since it overlaps with the peak of the CNT_f. In addition, it is observed that the width of the peaks in both compound increases with respect to the HAp, being greater in the CNT_f/HAp compound (100); It is expected that the crystal size will be smaller than that of the HAp and decrease in the following order HAp > CNT_f/HAp (36) > CNT_f/HAp (100).

4.3.3 TRANSMISSION ELECTRON MICROSCOPY (TEM)

In Figures 19 and 20 it is observed that the HAp particles are located in areas where the CNT_f are agglomerated, which seems to indicate that the HAp is supported on the nanotubes and not chemically bound to them. Also, it is observed that there is more quantity of HAp in the

CNTf/HAp system (36) than in the CNTf / HAp system (100), as obtained in the FTIR and DRX analyzes. The particles of HAp in these systems have a spherical shape, while the particles of HAp synthesized without the CNTf are stick-shaped. The average size of HAp particles in the CNTf/HAp system (36), shown in Figure 19-B, is 7.6 nm.

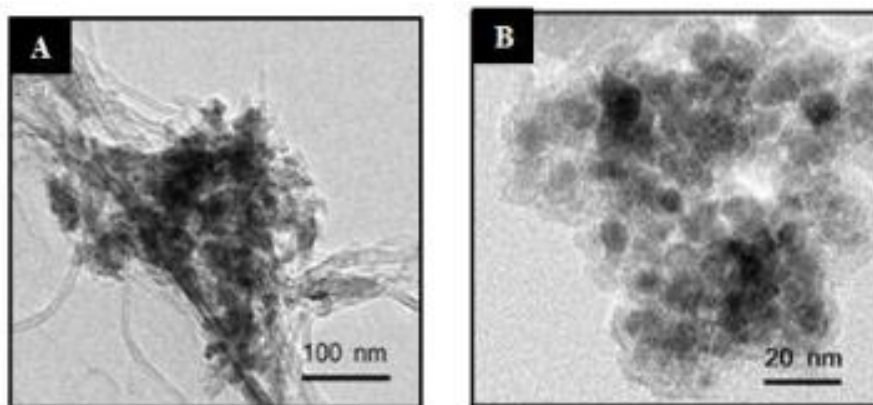


Figure 19. TEM-HR images of the CNT_f / HAp nanostructured system (36).

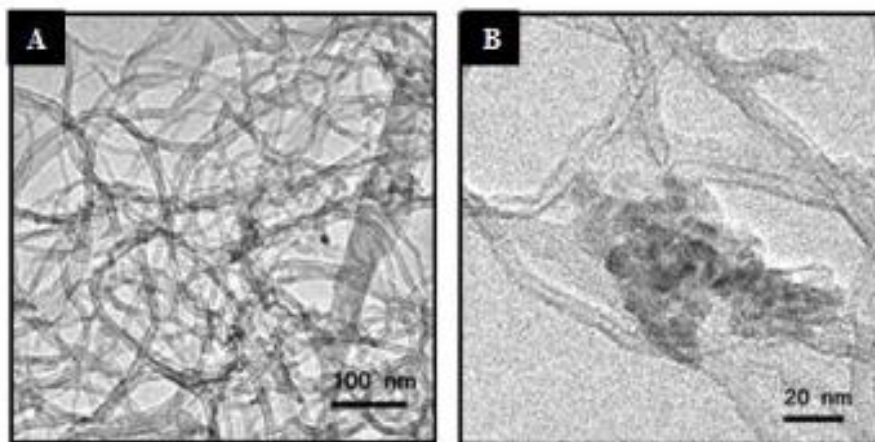


Figure 20. TEM-HR images of the CNT_f / HAp nanostructured system (100).

4.4 ELECTROCHEMICAL CHARACTERIZATION

In this thesis, $[\text{Fe}(\text{CN})_6]^{3-/4-}$ was used as benchmark redox system, to determine the electrochemical behavior of electrodes through cyclic voltammetry studies. Prior to start with the electrochemical characterization, in order to clean and active the surface of bare and modified 2H graphite electrodes, a cyclic voltammetry was potential scanned between -1.2 V and -1.5 V in 0.1 mol L⁻¹ PBS, at scan rate of 100 mV s⁻¹, during 25 cycles.

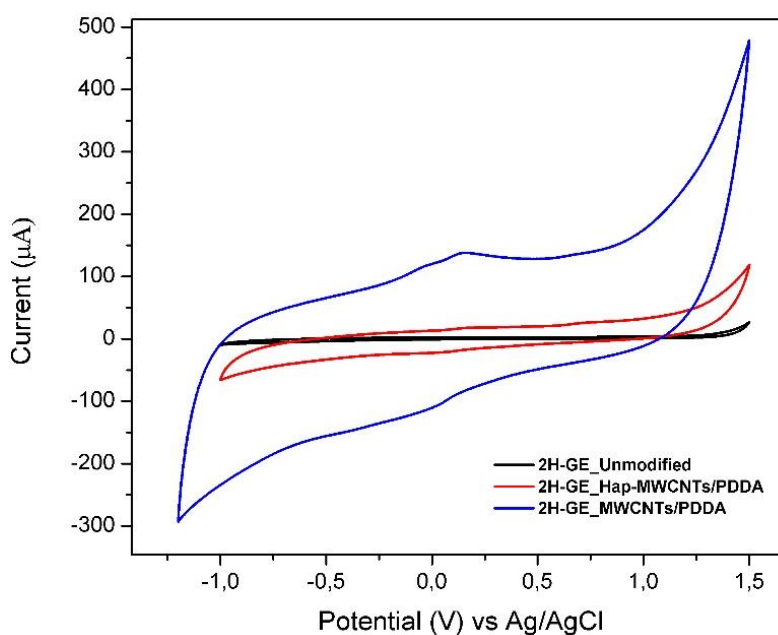


Figure 21. Cyclic voltammogram of bare and modified electrodes in 0.1 mol L⁻¹ PBS, at scan rate of 100 mV s⁻¹. Abbreviations: 2H-GE, 2H graphite electrode; HAp-MCNTs, multiwalled carbon nanotubes with hydroxyapatite nanoparticles; MWCNTs, multiwalled carbon nanotubes; PDDA [Poly(diallyldimethylammonium chloride)].

As illustrated Figure 21, there are not peaks showed on the cyclic voltammogram of bare and modified 2H graphite electrodes, in the potential range employed, due PBS solution is a standard solution, therefore no reduction and oxidation reactions have occurred.

4.4.1 ELECTROCHEMICAL BEHAVIOR OF 2H-GE ELECTRODE

Figure 22, represents the voltammetric curves of bare 2H graphite electrode (2H-GE_unmodified), recorded in the presence of the 4 mmol L⁻¹ K₃[Fe (CN)₆] solution containing 0.1 mol L⁻¹ PBS, in the potential range of + 0.2 to - 0.6 V, at different scan rates (v) from 20 to 120 mV s⁻¹. Two redox peaks well-defined are observed, related to the oxidation of Fe^{II} to Fe^{III} during the anodic scan, and reduction of Fe^{III} to Fe^{II} during cathodic scan [Fe (CN)₆⁴⁻ ⇌ Fe (CN)₆³⁻ + e⁻].

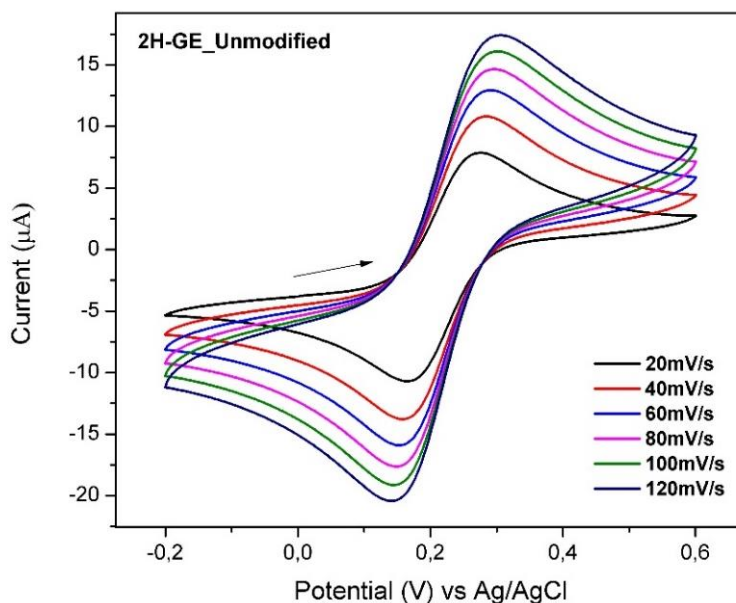


Figure 22. Cyclic voltammograms of 2H-GE recorded in 4mM K₃ [Fe (CN)₆] with phosphate buffer solution (pH = 7.4) at different scan rates. Abbreviations: 2H-GE, bare 2H graphite electrode.

The redox peaks are located at 0.2 V (versus Ag/AgCl) with an average peak separation potential (ΔE_p) around of 139 mV (vs. Ag/AgCl), at scan rates from 20 mV s⁻¹ to 120 mV s⁻¹. This value was far to the theoretical value expected for a one-electron transfer for reversible system which is 59 mV/n,⁶⁰ however, the ratio between the anodic and cathodic peak current (i_{pa}/i_{pc}), was closest to the ideal value of one, for reversible system,⁶⁰ therefore, we can say that the 2H graphite electrode has a quasi-reversible behavior.

Table 6. Electrochemical parameters obtained from cyclic voltammogram of 2H graphite electrode of 4 mM K₃ [Fe (CN)₆] containing in 0.1 M PBS, at different scan rates.

Scan rate (mV/s)	<i>i</i> _{pa} (μA)	<i>i</i> _{pc} (μA)	<i>i</i> _{pa} / <i>i</i> _{pc}	<i>E</i> _{pa} (V)	<i>E</i> _{pc} (V)	<i>E</i> _{p1/2} (V)	Δ <i>E</i> _p (V)
20	7.870	-10.708	0.734	0.275	0.166	0.220	0.109
40	10.812	-13.784	0.784	0.283	0.158	0.220	0.124
60	12.948	-15.905	0.814	0.290	0.153	0.222	0.136
80	14.660	-17.636	0.831	0.295	0.148	0.222	0.146
100	16.107	-19.134	0.841	0.300	0.144	0.222	0.156
120	17.422	-20.431	0.852	0.305	0.141	0.223	0.163

Abbreviations: *i*_{pa}-anodic peak current; *i*_{pc}-cathodic peak current; *E*_{pa}-anodic peak potential; *E*_{pc}-cathodic peak potential; *E*_{p1/2} - half-wave potential; Δ*E*_p -peak-to-peak separation.

According to data of Table 6, for 2H graphite electrode, it can be see that the values of *E*_{pa} and *E*_{pc} tend to more positive and negative potentials, respectively, and the Δ*E*_p increases with the increase of scan rate. That is to say, the effect of scan rate (*v*) has a great influence on the redox process at the surface of the electrode, which indicates a linear dependence between anodic and cathodic peaks current with the square root of scan rate (*v*)^{1/2}, as illustrated in the Figure 23 (A), which confirm the quasi-reversibility and also suggest a diffusion controlled redox reaction at the electrode surface 68. The mentioned relation can be expressed by following equations:

$$i_{pa} (\mu A) = 1.469 v^{1/2} (mV s^{-1})^{1/2} + 1.436, (R^2 = 0.9995) \quad (12)$$

$$i_{pc} (\mu A) = -1.494 v^{1/2} (mV s^{-1})^{1/2} - 4.203, (R^2 = 0.9993) \quad (13)$$

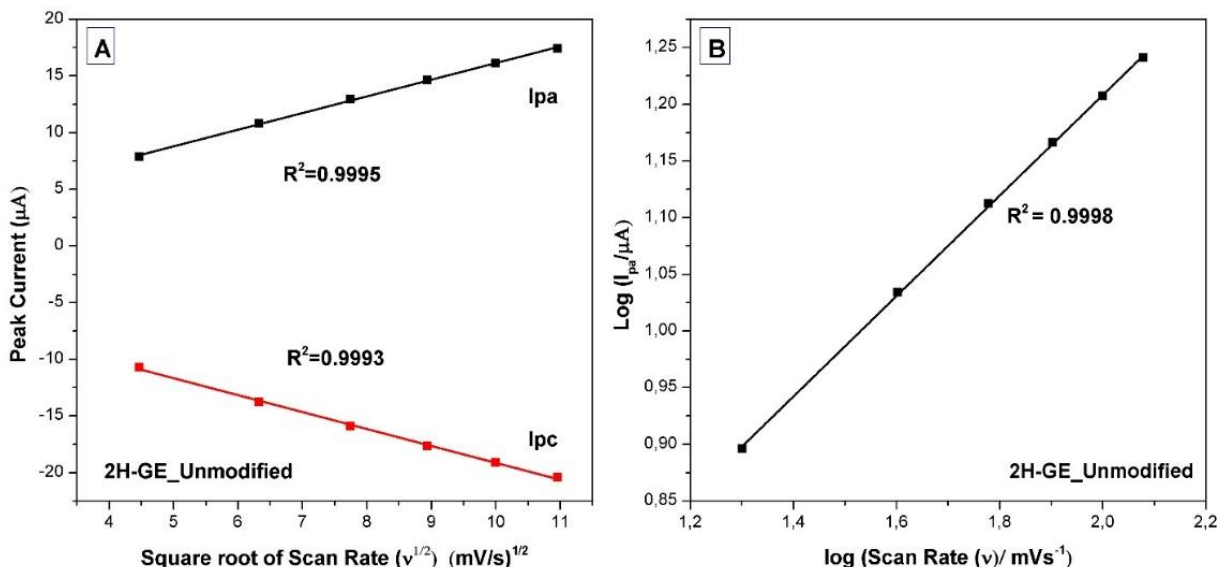


Figure 23. A) Plot of anodic and cathodic peak current and square root of scan rate, and B) Linear relationship of \log (anodic current, i_{pa}) with the \log (scan rate) for 2H graphite electrode unmodified.

Additionally, another test was carried out, to confirm that reaction is diffusion controlled at the surface electrode, which consist in a linear dependence of logarithm of anodic peak current ($\log i_{pa}$) with the logarithm scan rate ($\log v$), as illustrated in Figure 23 (B). The slope value of the straight line was 0.4431 with a correlation coefficient of 0.9998, which corresponding to the theoretical value of transfer coefficient ($\alpha = 0.5$) for the diffusion controlled process, according to Bard, Faulkner and co-workers.⁶⁰ The mentioned relation can be expressed by following equation:

$$i_{pa} (\mu\text{A}) = 0.4431 \log v (\text{mV s}^{-1}) + 0.3218, (R^2 = 0.9998) \quad (14)$$

The determination of electrochemical active surface area (A_e) was carried out using the Randles-Sevcik equation, for quasi-reversible electron transfer processes according to the following expression:⁶⁰

$$i_p = (2.65 \times 10^5) n^{3/2} A C D^{1/2} v^{1/2} \quad (15)$$

where i_p is peak current (A), constant (2.65×10^5) expressed in $C \text{ mol}^{-1} \text{ V}^{-1/2}$, n is electron stoichiometry ($n=1$, $K_3 [\text{Fe} (\text{CN})_6]$), A is the electrode area, D is diffusion coefficient ($7.69 \times 10^{-6} \text{ cm}^2 \text{ s}^{-1}$)⁶⁹, C is concentration of $K_3 [\text{Fe} (\text{CN})_6]$ (mol/cm^3), and v is scan rate (V/s). From the value of the slope of equation (12): $1.469 \mu\text{A mV}^{-1/2} \text{ s}^{-1/2}$, after of transformed to appropriated units, the electrochemical active surface active area (A_e) of 2H-graphite electrode was estimated to be 0.0158 cm^2 .

The ratio between electroactive surface area and geometrical area (A_e/A_{ge}), also called roughness factor, plays an important role for assessing material performance, which affects to electrochemical properties. High values proves that it has more exposed electrochemically active surface area, in this case the roughness factor was 0.5031.

4.4.2 ELECTROCHEMICAL BEHAVIOR OF MODIFIED ELECTRODES

The electrochemical characterization of modified electrodes were carried out by cyclic voltammetry based on potassium ferricyanide aqueous solution, as before. The modification of 2H graphite electrode implies coating its surface with MWCNTs and Hap-MWCNTs, with the purpose enhance the electrochemical properties of those electrodes by the use of carbon nanomateriales. From the Figure 24, it is possible to observe the typical redox peaks, corresponding to the $\text{Fe}^{3+}/\text{Fe}^{2+}$ redox couple. The principal parameters obtained of voltammograms and others calculated are recorded on the Table 7.

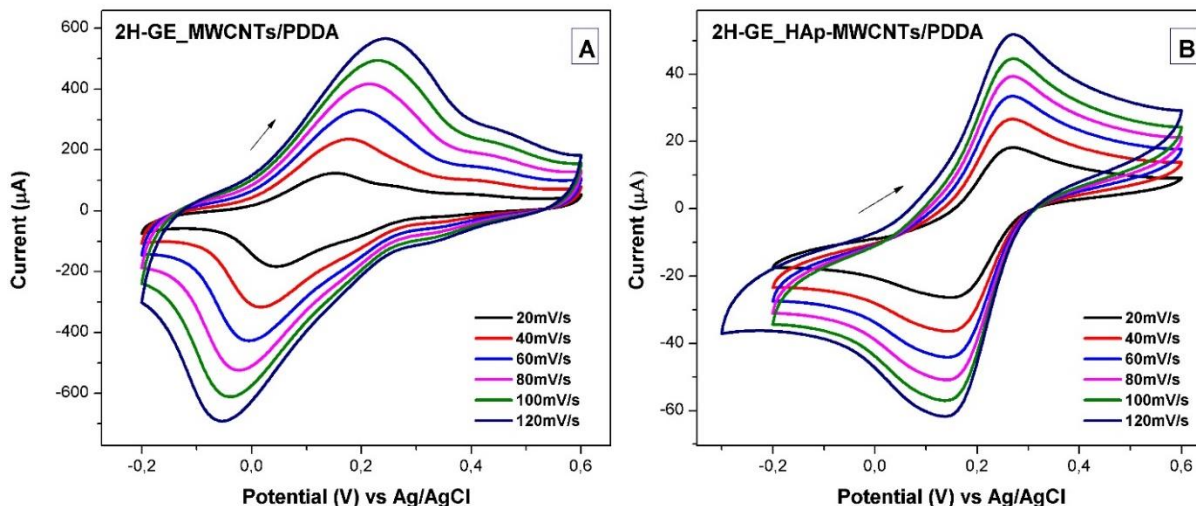


Figure 24. Cyclic voltammograms of 2Hgraphite electrode modified with A) MWCNTs and B) HAp-MWCNTs, immersed in 4 mM $K_3[Fe(CN)_6]$ solution with 0.1 M PBS (pH 7.4).

From Figure 24(A), the redox peaks for MWCNTs modified electrode are located at 0.096 V (vs. Ag/AgCl), with an average peak separation potential (ΔE_p) around 211 mV (vs. Ag/AgCl), meanwhile, for HAp-MWCNTs modified electrode are located at 0.204 V (vs. Ag/AgCl), with average ΔE_p of 129 mV (vs. Ag/AgCl), at scan rates from 20 $mV s^{-1}$ to 120 $mV s^{-1}$. Comparing these values, 2H-GE/HAp-MWCNTs leads to sharper peaks with a better reversibility [see Figure 24 (B)], due to lower potential peak separation, although, the values of both modifications are far from the theoretical value (59 mV/n). However, the ratio (i_{pa} / i_{pc}), for both modifications was close to one, therefore, both modifications present a quasi-reversible behavior.

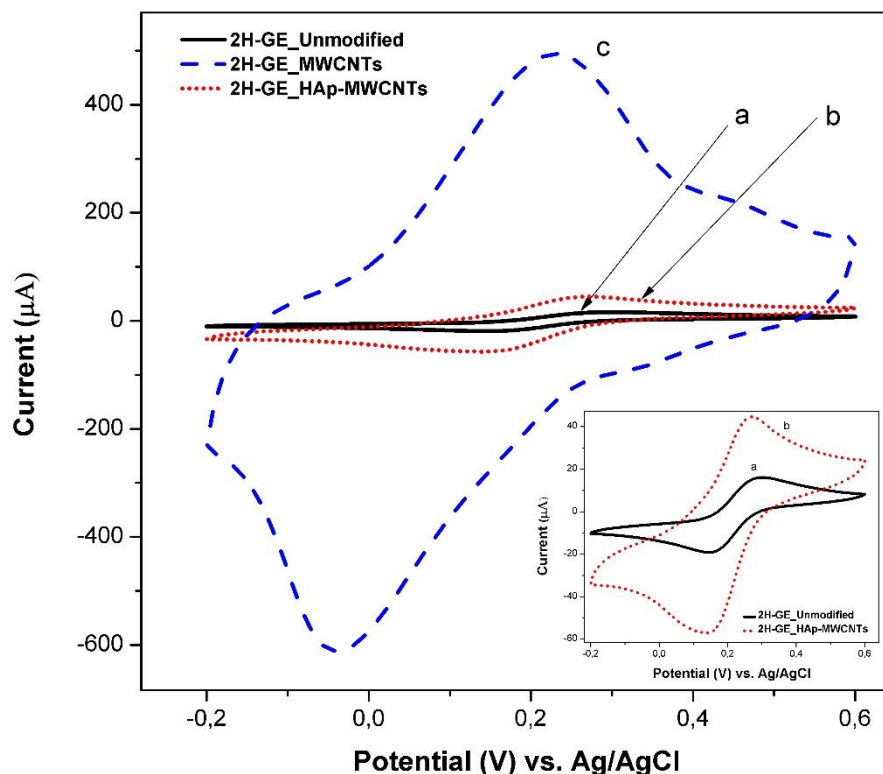


Figure 25. Cyclic Voltammograms of various electrodes immersed in 4 mmol L⁻¹ [Fe(CN)₆]^{3-/4-} with 0.1 mol L⁻¹ PBS recorded on a) bare 2H-GE, b) 2H-GE/HAp-MWCNTs, and c) 2H-GE/MWCNTs, at scan rate of 100 mVs⁻¹.

The analysis of cyclic voltammograms of the modified electrodes show to notorious, increment of anodic and cathodic peak currents in relation to the bare 2H-GE, at scan rate of 100 mVs⁻¹ (see Figure 25). The bare 2H graphite electrode presents a maximum of 16.107 μA and -19.134 μA for anodic and cathodic peaks current, however, 2H-GE/MWCNTs exhibited a higher redox peak current with a maximum of current of 494,445 μA and -611,572 μA for anodic and cathodic peaks, respectively, as compared to the modification with hydroxyapatite nanoparticles, which present a maximum of 44.628 μA and -57.037 μA for anodic and cathodic current peaks. The peak current increment accompanied with peak separation potential (ΔE_p) of 2H-GE/MWCNTs, suggest, an excellent electrocatalytic activity and surface area effect of MWCNTs material,¹⁸ that improves the current response of [Fe(CN)₆]^{3-/4-}. The increment of current 2H-

GE/HAp-MWCNTs indicated the hydroxyapatite nanoparticles undergo a faster electron transfer than 2H-GE, and more reversible 2H-GE/MWCNTs, this can be attributed to the porous structure of hydroxyapatite (HAp) which has a high adsorption capacity.^{29,70}

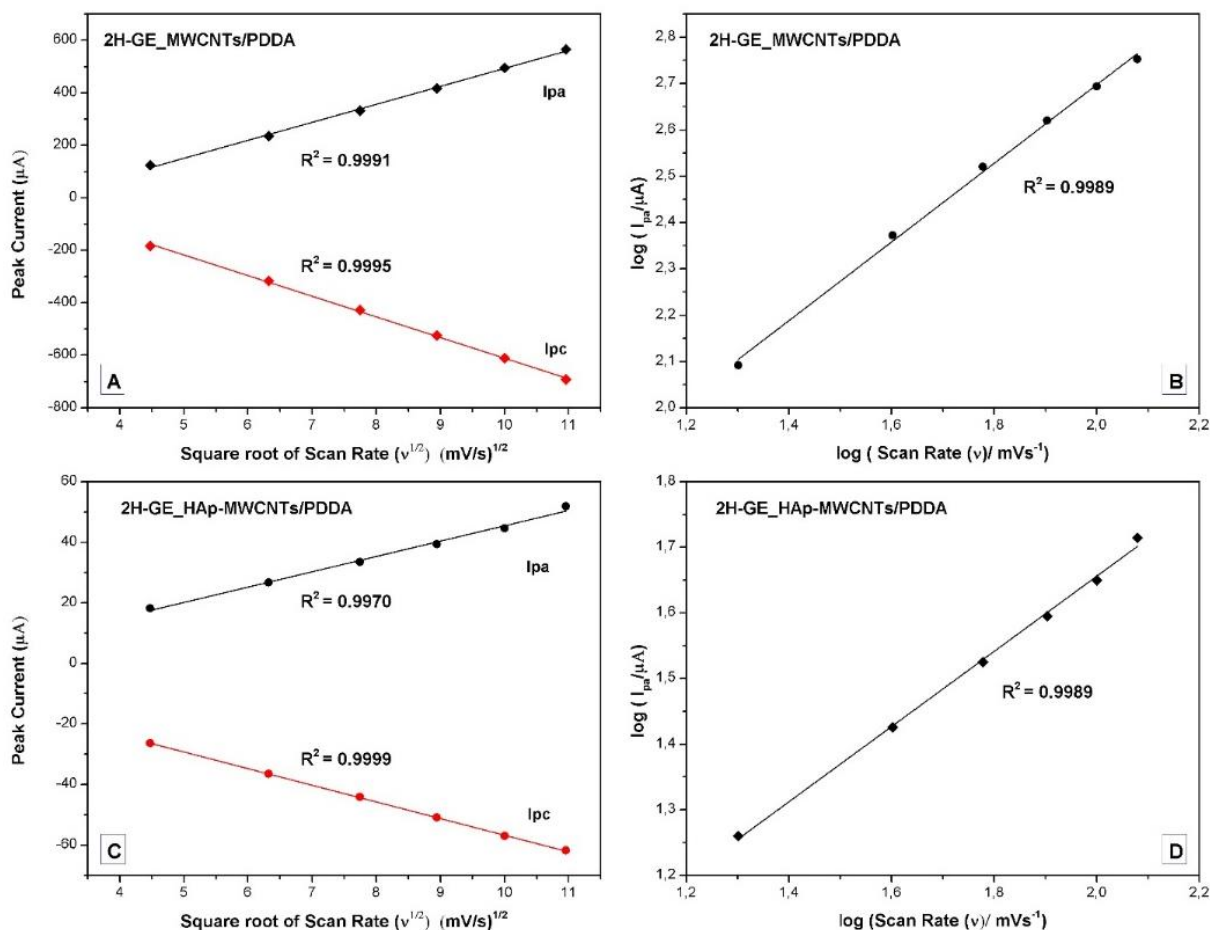


Figure 26. Plots: peak currents of 2H-GE/MWCNTs vs. a) square root of scan rate, b) log (scan rate), and peaks currents of 2H-GE/HAp-MWCNTs vs. c) square root of scan rate, d) log (scan rate).

The modified electrodes shown a linearly related with the square root of the scan rate in the range of 20 to 120 mV s^{-1} . which suggest a diffusion-controlled reaction, as illustrate the Figures 26 (A) and (C). The mentioned relation can be expressed by following equations:

- **For 2H-GE/MWCNTs:**

$$i_{pa} (\mu\text{A}) = 68.501 v^{1/2} (\text{mV s}^{-1})^{1/2} - 191.807, (R^2 = 0.9991) \quad (16)$$

$$i_{pc} (\mu\text{A}) = -78.683 v^{1/2} (\text{mV s}^{-1})^{1/2} + 176.137, (R^2 = 0.9995) \quad (17)$$

- **For 2H-GE/HAp-MWCNTs:**

$$i_{pa} (\mu\text{A}) = 5.063 v^{1/2} (\text{mV s}^{-1})^{1/2} - 5.187, (R^2 = 0.9970) \quad (18)$$

$$i_{pc} (\mu\text{A}) = -5.498 v^{1/2} (\text{mV s}^{-1})^{1/2} - 1.718, (R^2 = 0.9999) \quad (19)$$

Analogous, a linear relationship is observed between $\log(i_{pa})$ and $\log(v)$ on the Figures 26 (B) and (D), and the corresponding equations and correlation coefficients are by following equations:

- **For 2H-GE/MWCNTs:**

$$i_{pa} (\mu\text{A}) = 0.848 \log v (\text{mV s}^{-1}) + 0.999, (R^2 = 0.9989) \quad (20)$$

- **For 2H-GE/HAp-MWCNTs:**

$$i_{pa} (\mu\text{A}) = 0.509 \log v (\text{mV s}^{-1}) + 0.573, (R^2 = 0.9989) \quad (21)$$

The slopes value of 0.848 is far of theoretical diffusion value of 0.5, corresponding to the 2H-GE/MWCNTs, and the value of 0.509 is close to the theretical and a diffusion controlled process, corresponding to the 2H-GE/HAp-MWCNTs.60

The electrochemical active surface area (A_e) for each modified electrodes were obtained from the slope of equation (16) for 2H-GE/MWCNTs, and equation (18) for 2H-GE/HAp-MWCNTs, using the Randles-Sevcik equation (15), such results, were 0.7412 cm^2 and 0.0547

cm², respectively. The roughness factor for each modified electrode were 23.60 and 1.742, respectively. The results are in agreement with the higher background current observed for 2H-GE/MWCNTs, due that have higher electroactive area with more defects of MWCNTs on the surface of electrode, that improve the electrochemical performance.

Table 7. Electrochemical parameters obtained from cyclic voltammogram of 2H graphite electrode modified with MWCNTs and HAp-MWCNTs of 4mM K₃ [Fe (CN)₆] containing in 0.1 M PBS, at different scan rates.

2H-GE/MWCNTs/PDDA							
Scan rate (mV/s)	i_{pa} (μA)	i_{pc} (μA)	i_{pa}/i_{pc}	E_{pa} (V)	E_{pc} (V)	E_{p(1/2)} (V)	ΔE_p (V)
20	123.443	-183.258	0.673	0.153	0.043	0.098	0.110
40	235.656	-316.406	0.744	0.178	0.017	0.097	0.161
60	331.390	-427.337	0.775	0.197	-0.004	0.096	0.201
80	416.748	-524.291	0.794	0.214	-0.021	0.096	0.235
100	494.445	-611.572	0.808	0.229	-0.036	0.096	0.265
120	565.795	-691.833	0.817	0.241	-0.053	0.094	0.294
2H-GE/HAp-MWCNTs/PDDA							
Scan rate (mV/s)	i_{pa} (μA)	i_{pc} (μA)	i_{pa}/i_{pc}	E_{pa} (V)	E_{pc} (V)	E_{p(1/2)} (V)	ΔE_p (V)
20	18.200	-26.385	0.689	0.271	0.146	0.208	0.125
40	26.672	-36.431	0.732	0.268	0.144	0.206	0.124
60	33.483	-44.146	0.758	0.268	0.141	0.204	0.127
80	39.370	-50.903	0.773	0.271	0.139	0.205	0.132
100	44.628	-57.037	0.782	0.268	0.136	0.202	0.132
120	51.818	-61.767	0.838	0.271	0.136	0.203	0.135

Abbreviations: *i_{pa}*-anodic peak current; *i_{pc}*-cathodic peak current; *E_{pa}*-anodic peak potential; *E_{pc}*-cathodic peak potential; *E_{1/2}* - half-wave potential; *ΔE_p* -peak-to-peak separation; 2H-GE, 2H graphite electrode; HAp, Hydroxyapatite; MWCNTs, Multiwalled carbon nanotubes.

4.4.3 ELECTROCHEMICAL BEHAVIOR OF PRUSSIAN BLUE FILM

Once the Prussian Blue (PB) film was electrodeposited at the surface of modified 2H graphite electrodes, during 60 s, the films requires of an electrochemically activation by cyclic scan in the same supporting electrolyte (0.1 M HCl +0.1 M KCl), in the potential range of -150

mV and +500 mV, at a scan rate of 50 mVs^{-1} , with the purpose of growth and stabilizing the Prussian Blue film. Figure 27, represents a typical cyclic voltammograms obtained after of electrodeposition of Prussian Blue,⁷¹ for MWCNTs [Figure 27(A)] and HAp-MWCNTs modified electrodes [Figure 27(B)]. A couple a redox peak appeared located at 0.179 V (vs. Ag/AgCl) for MWCNTs/PB modified electrode and at 0.152 V (vs. Ag/AgCl) for HAp-MWCNTs/PB modified electrode, values according to the literature report^{43,71}. The redox peaks corresponding to redox conversion between Prussian Blue (PB, $\text{K}_2\text{Fe}^{\text{III}}[\text{Fe}^{\text{II}}(\text{CN})_6]$) and Prussian White (PW, $\text{K}_2\text{Fe}^{\text{II}}[\text{Fe}^{\text{II}}(\text{CN})_6]$) its reduced form, according to the reversible equation (1).

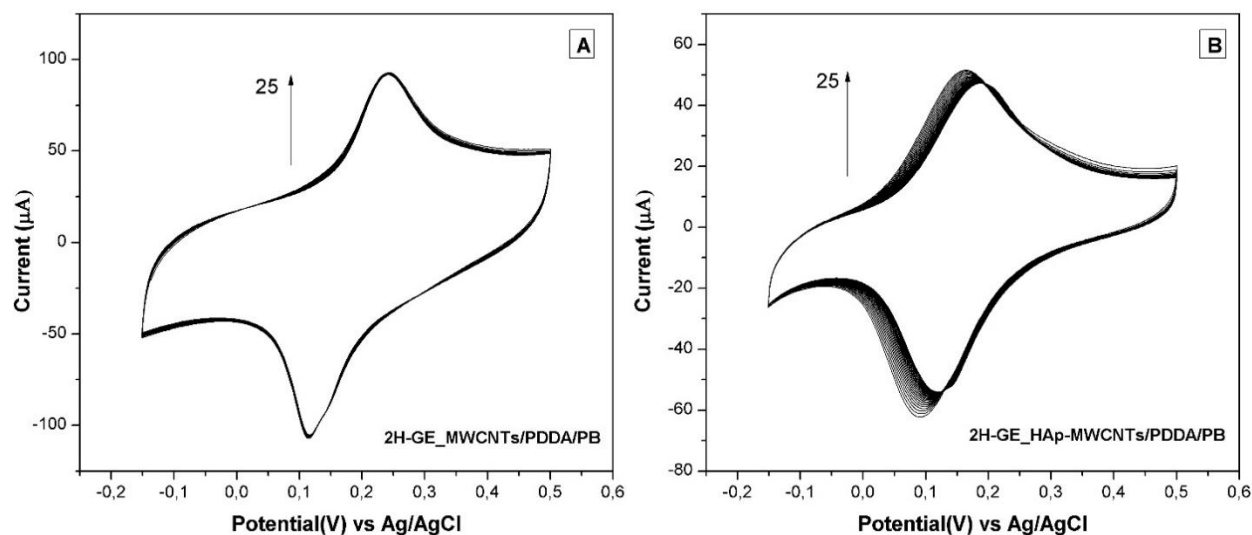


Figure 27. Cyclic voltammograms of Prussian Blue films activated in 0.1 M HCl + 0.1 M KCl solution on modified graphite electrode with A) MWCNTs, and B) HAp-MWCNTs.

Figure. 27(B), represents the cyclic voltammogram of the PB-HAp/MWCNT-modified electrode, which presents a lower potential peak separation ΔE_p of 70.8 mV (vs. Ag/AgCl), in comparison with the PB-MWCNT-modified electrode which reaches 124 mV (vs. Ag/AgCl). The lower value of ΔE_p indicates a better reversibility with a fast charge transfer in the modified film occurs. This can be attribute to the high capacity of adsorption of hydroxyapatite nanoparticles⁶ and the good electrochemical conductivity of multiwalled carbon nanotubes.⁷²

The maximum PB-film growth onto the surface of modified electrodes was obtained until reaches 25 cycles in the supporting electrolyte, where exhibited sharp peak currents indicating a regular structure of the inorganic polycrystal. The highest current peaks correspond to the MWCNTs/PB modified electrode, with values of 91.766 μA and -105.244 μA for anodic and cathodic peaks, respectively, meanwhile, HAp-MWCNTs/PB modified electrode, reaches 47.296 μA for anodic peak and - 54.092 μA for cathodic peak. Afterwards of 25 cycles, no decrease in peaks current and no expressive changes on the cyclic voltammogram obtained, therefore, this indicates a good adsorption of PB at the surface of electrode,⁷³ and as results a stable transition between PW and PB. According to the literature that follows the same procedure to electrodeposition and activation the PB-films, estimated the amount of deposited Prussian Blue about to $\sim 6 \text{ nmol cm}^2$, if a transfer of 4 electrons per unit cell is assumed.⁷⁴

As PB-films contain an average of 14-16 water molecules,³⁹ which affect the conductivity and stability of PB, therefore, these require of a dried at long time to removed it. The news modified electrodes were washing with distilled water and dried during 30 min at 50°C in an oven. Finally, 10 μL of PDDA was pipetted onto the surface of the modified electrodes, and dried at 50°C for 10 min. The PDDA maintaining the electrostatic force between its charged chains and cyanide groups, and presents a reservoir of well-bound PB.⁷⁵ Then, was stored at room temperature and dry conditions, until use for hydrogen peroxide determination. At this step, we can say that the electrochemical sensors are assembly.

4.5 STABILIZATION OF ELECTROCHEMICAL SENSOR

Before submitting the electrochemical sensors to the detection of hydrogen peroxide, the stability of sensors was verified by studying its electrochemical behavior in a blank solution of 0.1 M of PBS at pH 7.4, under potential range of -150 mV and +500 mV, scan rates of 50, 100 and 120 mV/s, during 25 cycles.

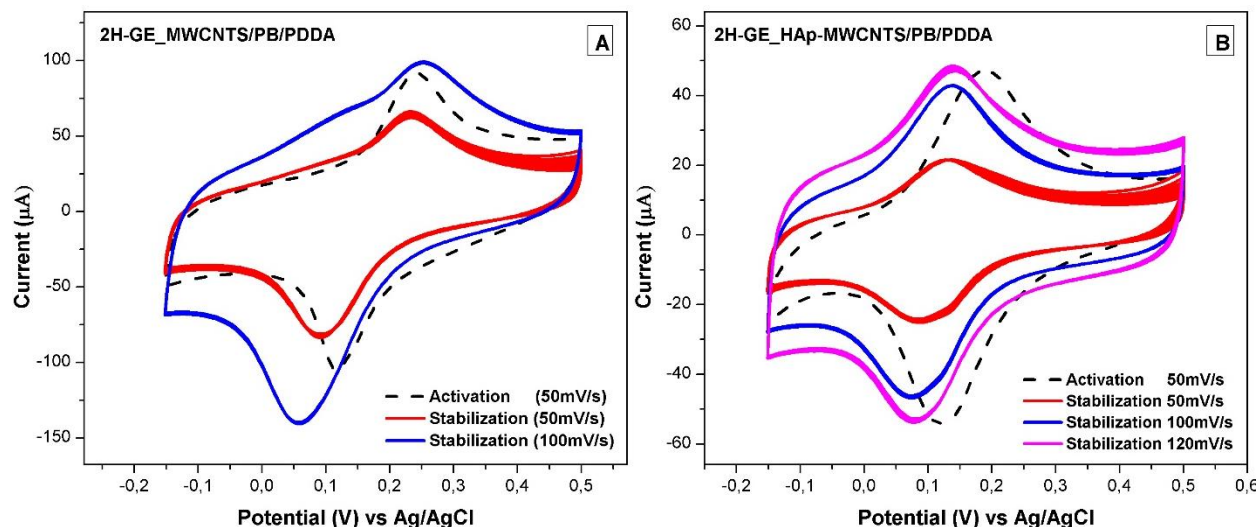


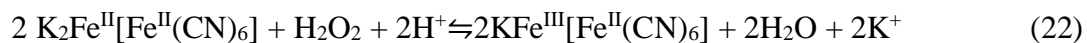
Figure 28. Cyclic voltammograms showing the current responses of A) MWCNTs/PB, and B) HAp-MWCNTs/PB modified electrodes in 0.1 M PBS, at alkaline pH of 7.4, at different scan rates.

Figure 28(B), shows the response of HAp-MWCNTs/PB modified electrode in PBS at pH conditions of 7.4. The redox peaks of PB were slightly altered, the values of E_{pa} and E_{pc} , shift negatively, meanwhile, the peak currents increase as increasing the scan rate, maintaining the shape of redox peaks at 0.108 V (vs. Ag/AgCl) and ΔE_p decreases at 61.03 mV (vs. Ag/AgCl), at 120 mV s^{-1} . These results indicates that HAp-MWCNTs/PB modified electrode has high stability, with a high electron transfer between PB and the HAp-MWCNTs, without damage in the structure of PB, at pH conditions of 7.4. This can be explained by the high capacity of adsorption and the higher surface-area of hydroxyapatite nanoparticles, where the Prussian blue was electrodeposited. The voltammogram of MWCNTs/PB modified electrode [see Figure 28 (A)], we can observed a notorious change on the redox peak of PB, when the anodic peak tend to disappear, at scan rate of 100 mVs^{-1} , while the cathodic peak increasing. This can be attributed to the presence of OH^- ions, which can leading to break the Fe-(CN)-Fe bonds, hence solubilizing PB,⁴⁹ therefore the sensor is less stable at pH conditions of 7.4.

4.6 RESPONSE OF THE MODIFIED ELECTRODES TO H₂O₂

The behavior of different modifications of 2H graphite electrode toward hydrogen peroxide reduction was carried out by cyclic voltammetry, as illustrated in Figure 29. The voltammetric response was analyzed in the presence of 1 mM H₂O₂ in 0.1 M PBS (pH = 7.4), at a potential range from -1 V to +0.5 V (vs. Ag/AgCl) with a scan rate of 50 mVs⁻¹. As can be seen from Figure 29: a) the modification of 2H-GE with hydroxyapatite nanoparticles presents a reduction current peak located at -0.42 V (vs. Ag/AgCl) with a slightly reduced current response, which indicates the electrocatalytic activity of H₂O₂, meanwhile, b) the modification with MWCNTs, the peak current had almost disappeared, due to MWCNTs are not good electrocatalysts for reducing H₂O₂,⁷² including c) its modification with PB which did not observe a remarkable peak and current response, at a lower concentration of H₂O₂. However, d) the modification with HAp-MWCNTs/PB shows a reduction current peak located at -0.35 V (vs. Ag/AgCl) with a moderate current response. The magnitude of the electrochemical response at these modified electrodes increases in the following order: HAp-MWCNTs/PB > HAp-MWCNTs > MWCNTs > MWCNTs/PB.

According to the results, we can say that hydroxyapatite nanoparticles could rapidly catalyze the reaction at low potentials, due to their zeolite structure which may allow the diffusion of small molecules into the lattices, such as O₂ and H₂O₂.⁴² Hence, this indicates that modifications of 2H-GE with HAp-MWCNTs and with PB show synergistic effects and can be sensitively detected by cyclic voltammetry in the presence of H₂O₂. The electrocatalytic mechanism of Prussian Blue for H₂O₂ reduction could be expressed as follows:



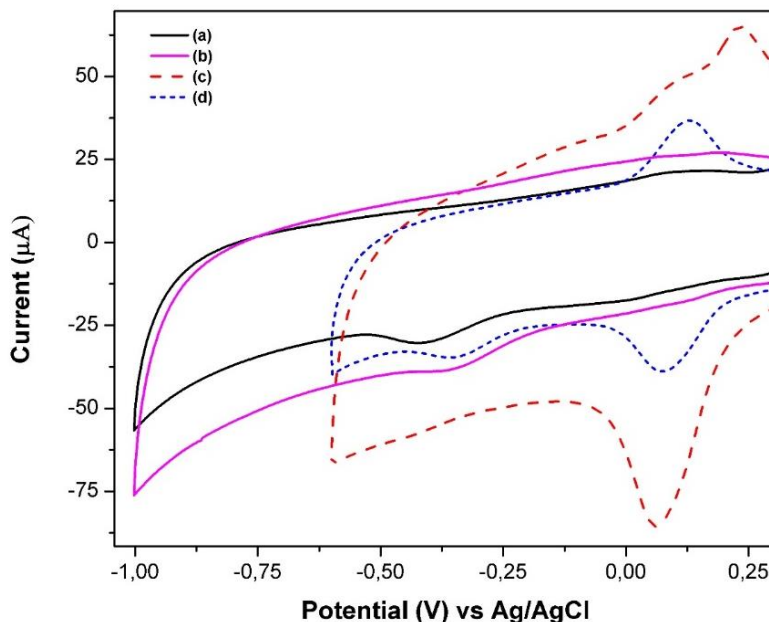


Figure 29. Cyclic Voltammograms of 2H-GE modified by a) HAp-MWCNTs, b) MWCNTs, c) MWCNTs/PB and d) HAp-MWCNTs/PB in 0.1 M PBS in 1mM H_2O_2 , at pH 7.4. Scan rate of 50 mVs^{-1} .

4.7 VOLTAMMETRIC DETECTION OF HYDROGEN PEROXIDE

The tests of the electrocatalytic reduction of H_2O_2 at the PB modified electrodes were carried out by cyclic voltammetry, in PBS solution at pH 7.4 in presence of different concentrations of hydrogen peroxide, since 1mM to 10 mM. Figure 30, shows the response of MWCNTs/PB modified electrode at the reduction of hydrogen peroxide, where can see two pairs of anodic and cathodic peak (I_{pa1}/I_{pc1}) and (I_{pa2}/I_{pc2}), located at 0.19 V and 0.7 V (vs Ag/AgCl), respectively. The first redox peak corresponds to the reduction of PB to PW at negative potentials [equation (1)], and the second to the oxidation of PB to Prussian Yellow or Berlin Green at positive potentials [equations 2 and 3]. However, appear another cathodic peak, proximate to the reduction peak of PB, located at 0.31V (vs Ag/AgCl) which indicates the electrocatalytic reduction of H_2O_2 .⁷⁶ The inset plot of the Figure 30, shows the linear relationship between the reduction peak current of hydrogen peroxide with its corresponding concentration. As can be seen, the sensor (MWCNTs/PB modified electrode), only can detect concentration since 5 mM to 10

mM, without current response at lower concentrations. Additionally, we expected a catalytic behavior of PB, where the cathodic peaks increase and the anodic peaks decrease as increasing the concentration of H_2O_2 , however, this not occur, which explains the lower peak current response for the reduction of hydrogen peroxide. The limit of detection (LOD), linear range and sensitivity were obtain from inset plot. Hence, the sensor shows a good linearity between 5 to 10 mM with a LOD of 2.6 mM ($\text{LOD}=3\times\text{SD}/\text{slope}$), limit of quantification ($\text{LOQ}=10\times\text{SD}/\text{slope}$) of 7.8 mM, and a sensitivity of $110.17 \mu\text{A mM}^{-1}\text{cm}^{-2}$.

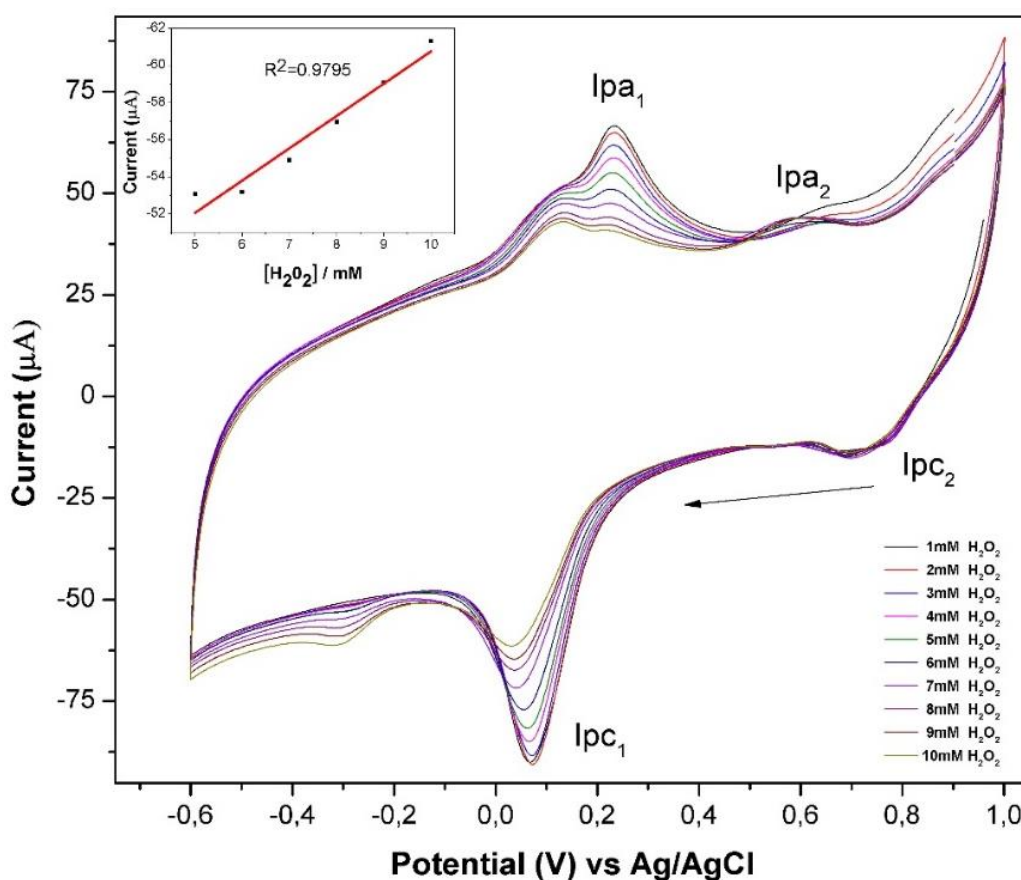


Figure 30. Voltammetric response of 1.0-10mM H_2O_2 at MWCNTs/PB modified electrode, at scan rate of 50 mV s^{-1} . Inset: Plot of response current versus H_2O_2 concentration.

The cyclic voltammogram of Figure 31, show the catalytic behavior of HAp-MWCNTs/PB modified electrode at the reduction of hydrogen peroxide. As seen before, two

pairs of anodic and cathodic peak ($I_{pa'1}/I_{pc'1}$) and ($I_{pa'2}/I_{pc'2}$) are presents on the voltammogram without shape variations on the peaks, correspondig to the reduction and oxidation form of PB. As evidenced, the reduction peak of H_2O_2 appear at -0.35 V (vs. Ag/AgCl).⁷⁶ According to the inset plot, the HAp-MWCNT electrode detects peroxide within the entire studied concentration range from 1 to 10 mM, with a calculated LOD of $230 \mu M$ and LOQ $780 \mu M$. The sensivity of the electrode was $119.77 \mu A \text{ mM}^{-1} \text{ cm}^{-2}$.

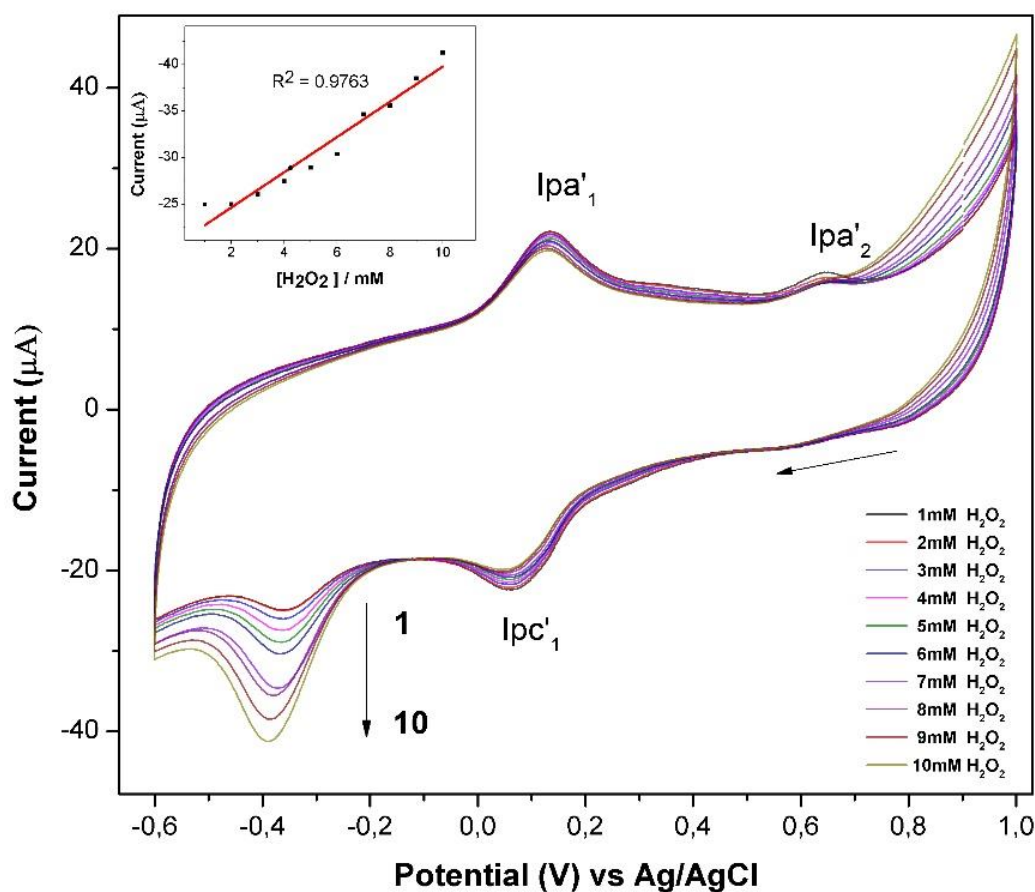


Figure 31. Voltammetric response of 1.0-10mM H_2O_2 at HAp-MWCNTs/PB modified electrode, at scan rate of 50 mV s^{-1} . Inset: Plot of response current versus H_2O_2 concentration.

The results are summarized in the Table 8, where the Hap-MWCNT/PB modified electrode detects peroxide within the entire studied concentration range from 1 to 10mM with a calculated LOD of 230 μM , LOQ 780 μM , and a sensitivity of 119.77 $\mu\text{A mM}^{-1}\text{cm}^{-2}$, while the MWCNT/PB modified electrode is only able to detect concentrations above 5mM with a lower LOD of 2.3 mM and LOQ of 1.02 mM with a sensitivity of 110.72 $\mu\text{A mM}^{-1}\text{cm}^{-2}$.

Table 8. Analytical performance characteristics of a number of Prussian blue and Hydroxyapatite modified electrodes for H_2O_2 detection.

Modified electrode	Linear response range	Sensitivity	LOD	LOQ	Technique	Ref
2H-GE/MWCNT/PB	5-10 (mM)	110.72 $\mu\text{A mM}^{-1}\text{cm}^{-2}$	2.3 mM	1.02 mM	CV	This Work
SPE/PBNPs(15nm)/MWCNT	0.001-4.5 (mM)	762 $\mu\text{A mM}^{-1}\text{cm}^{-2}$	0.2 μM	-----	Amperometric	[71]
Au/PB-MWCNTs	1 μM -5mM	856 $\mu\text{A mM}^{-1}\text{cm}^{-2}$	23nM	-----	Amperometric	[73]
2H-GE/HAp-MWCNT/PB	1-10 (mM)	119.77 $\mu\text{A mM}^{-1}\text{cm}^{-2}$	230 μM	780 μM	CV	This work
GC/HRP-HAP	5 μM -to-0.82 mM	6.75 mAM^{-1}	0.1 μM	-----	Amperometric	[5]
GC/RGO/HAp/GOx	0.1-11.5 (mM)	16.9 $\mu\text{A mM}^{-1}\text{cm}^{-2}$	0.03 mM	-----	Amperometric	[35]

Abbreviations: SPE-Screen-Printed Electrode; RGO-Reduced graphene oxide

There are exist literature reported for electrochemical sensors, that use Hydroxyapatite nanoparticles and also Prussian blue. For example, Zhang et al. [5] achieved a LOD of $0.1 \mu\text{M}$ and a sensitivity of 6.75 mA M^{-1} . Bharath et al. [35] achieved an analytical range from 0.1 to 11.5 mM by using composite of HAp nanoparticles and Glucose oxidase (GOx). The analytical parameters of 2H-GE/MWCNT/PB sensor, are far to the reported, however, we can see that the used of nanoparticles of hydroxyapatite allow an higher linear range of detection in all cases. This can be attribute to the high surface area, high adsorption and the electrocatalytic properties that have the hydroxyapatite to reduce the hydrogen peroxide. On the case of Prussian Blue, Li et al.[71] achieved a lower LOD $0.2 \mu\text{M}$ with a sensitivity of $762 \mu\text{A mM}^{-1}\text{cm}^{-2}$, with the used of Prussian blue nanoparticles into a screen printed electrode, and for its big surface area is notorious the high value of sensitivity. The sensitivity of $110.72 \mu\text{A mM}^{-1}\text{cm}^{-2}$ of 2H-GE/MWCNT/PB sensor, is far to the reported. However, we can see the values reported, should be higher, but a low limit of detection. In our case the sensor's responses at lower concentration ranges is still under study and shows promising results.

CHAPTER 5

CONCLUSIONS

In conclusion, cyclic voltammetry demonstrates that the graphite electrode fabricated based on commercial 2H pencil graphite lead, provides the require reversibility for redox system $[\text{Fe}(\text{CN})_6]^{3-/4-}$, an important aspect for the qualitative and quantitative analysis. The modification of its surface by carbon nanomaterials allow improves its electrochemical behavior, in our case the HAp-MWCNTs improves the reversibility, increasing the electron transfer, due to the high area and adsorption capacity of hydroxyapatite nanoparticles. The incorporation of Prussian Blue as electrocatalytic transducer facilitate the electron transfer and the selectivity toward reduction of hydrogen peroxide. The multi-layer procedure of assembly has allows to obtain a stable electrochemical sensor due the electrostatic interactions between layers. The final sensor obtained called HAp-MWCNTs/PB showed a good electrocatalytic response to the reduction of hydrogen peroxide with a sensitivity of $119.77 \mu\text{A mM}^{-1}\text{cm}^{-2}$ in a range of concentration of 1 to 10 mM and a correlation coefficient of ($R^2 = 0.9763$) with a detection limit of $230 \mu\text{M}$. The developed sensor represents a simple, robust and reliable means of sensing H_2O_2 which avoids long and complex fabrication processes and is suitable for large scale mass production and has many potential applications in environmental, biomedicine, and industrial monitoring.

REFERENCES

- (1) Chen, W.; Cai, S.; Ren, Q.; Wen, W.; Zhao, Y. Recent Advances in Electrochemical Sensing for Hydrogen Peroxide: A Review †. **2012**, 49–58. <https://doi.org/10.1039/c1an15738h>.
- (2) Ahammad, A. J. S. Biosensors & Bioelectronics Hydrogen Peroxide Biosensors Based on Horseradish Peroxidase and Hemoglobin. **2013**, 1–11. <https://doi.org/10.4172/2155-6210.S9-001>.
- (3) Rivas, G. A.; Rubianes, M. D.; Rodríguez, M. C.; Ferreyra, N. F.; Luque, G. L.; Pedano, M. L.; Misorcia, S. A.; Parrado, C. Carbon Nanotubes for Electrochemical Biosensing. *Talanta* **2007**, 74 (3), 291–307. <https://doi.org/10.1016/j.talanta.2007.10.013>.
- (4) Nanotubes-, M. C.; Acid, L.; Han, H. S.; You, J.; Jeong, H.; Jeon, S. Electrochemical Sensing of H₂O₂ by the Modified Electrode with Pd Nanoparticles On. **2014**, 4050–4057. <https://doi.org/10.1166/jnn.2014.8258>.
- (5) Zhang, M.; Yuan, R.; Chai, Y.; Li, W.; Zhong, H.; Wang, C. Glucose Biosensor Based on Titanium Dioxide-Multiwall Carbon Nanotubes-Chitosan Composite and Functionalized Gold Nanoparticles. *Bioprocess Biosyst. Eng.* **2011**, 34 (9), 1143–1150. <https://doi.org/10.1007/s00449-011-0565-4>.
- (6) Ferraz, M. P.; Monteiro, F. J.; Manuel, C. M. Hydroxyapatite Nanoparticles: A Review Of. **2004**, 74–80.
- (7) Karyakin, A. A.; Karyakina, E. E.; Gorton, L. Amperometric Biosensor for Glutamate Using Prussian Blue-Based “ Artificial Peroxidase ” as a Transducer for Hydrogen Peroxide. **2000**, 72 (7), 1720–1723.
- (8) Ricci, F.; Palleschi, G. Sensor and Biosensor Preparation , Optimisation and Applications of Prussian Blue Modified Electrodes. **2005**, 21, 389–407. <https://doi.org/10.1016/j.bios.2004.12.001>.
- (9) Thevenot, D.; Toth, K.; Durst, R.; Wilson, G.; Thevenot, D.; Toth, K.; Durst, R.; Wilson,

- G. Electrochemical Biosensors : Recommended Definitions and Classification To Cite This Version : HAL Id: Hal-00862855 ELECTROCHEMICAL BIOSENSORS : RECOMMENDED. **2013**.
- (10) Urban, G. A. Florinel-Gabriel Banica: Chemical Sensors and Biosensors: Fundamentals and Applications. *Anal. Bioanal. Chem.* **2013**, 405 (16), 5365–5366. <https://doi.org/10.1007/s00216-013-6870-9>.
 - (11) Ali, J.; Najeeb, J.; Ali, M. A.; Aslam, M. F.; Raza, A. Biosensors & Bioelectronics Biosensors : Their Fundamentals , Designs , Types and Most Recent Impactful Applications : A Review. **2017**, 8 (1), 1–9. <https://doi.org/10.4172/2155-6210.1000235>.
 - (12) Union, I.; Pure, O. F.; Chemistry, A. COMMISSION ON GENERAL ASPECTS OF ANALYTICAL CHEMISTRY AND CHEMICAL SENSORS. **1991**, 63 (9), 1247–1250.
 - (13) Koyun, A.; Ahlatc, E.; İ, Y. K. Biosensors and Their Principles. **1962**.
 - (14) Mungroo, N. A.; Neethirajan, S. Biosensors for the Detection of Antibiotics in Poultry Industry—A Review. **2014**, 472–493. <https://doi.org/10.3390/bios4040472>.
 - (15) Brett, C. M. A. Electrochemical Sensors for Environmental Monitoring . Strategy and Examples *. **2001**, 73 (12), 1969–1977.
 - (16) Saifuddin, N.; Raziah, A. Z.; Junizah, A. R. Carbon Nanotubes : A Review on Structure and Their Interaction with Proteins. **2013**, 2013.
 - (17) Ajayan, P. M. Nanotubes from Carbon. **1999**.
 - (18) Sinha, N.; Ma, J.; Yeow, J. T. W. Carbon Nanotube-Based Sensors. *J. Nanosci. Nanotechnol.* **2006**, 6 (3), 573–590. <https://doi.org/10.1166/jnn.2006.121>.
 - (19) Sinha, N.; Member, S.; Yeow, J. T. Carbon Nanotubes for Biomedical Applications. **2005**, 4 (2), 180–195.
 - (20) Rashid, H.; Ralph, S. F. Carbon Nanotube Membranes : Synthesis , Properties , and Future Filtration Applications. **2017**. <https://doi.org/10.3390/nano7050099>.

- (21) Yarlagadda, G.; Solasa, G.; Boanapalli, R.; Paladugu, P. Three-Dimensional Finite Element (FE) Model for Armchair and Zigzag Type Single-Walled Carbon Nanotubes. **2013**, *3* (5), 1–9.
- (22) Jeon, I.; Chang, D. W. Functionalization of Carbon Nanotubes. **1991**.
- (23) Veerapandian, M.; Yun, K. Functionalization of Biomolecules on Nanoparticles : Specialized for Antibacterial Applications. **2011**, 1655–1667. <https://doi.org/10.1007/s00253-011-3291-6>.
- (24) Uwimbabazi, E.; Mukasekuru, M. R.; Sun, X. Glucose Biosensor Based on a Glassy Carbon Electrode Modified with Multi-Walled Carbon Nanotubes-Chitosan for the Determination of Beef Freshness. *Food Anal. Methods* **2017**, *10* (8), 2667–2676. <https://doi.org/10.1007/s12161-017-0793-6>.
- (25) Liu, H.; Qian, X.; Wang, S.; Li, Y.; Song, Y.; Zhu, D. Ultra-Sensitivity Glucose Sensor Based on Field Emitters. *Nanoscale Res. Lett.* **2009**, *4* (10), 1141–1145. <https://doi.org/10.1007/s11671-009-9372-0>.
- (26) Hwang, D. W.; Lee, S.; Seo, M.; Chung, T. D. Recent Advances in Electrochemical Non-Enzymatic Glucose Sensors – A Review. *Anal. Chim. Acta* **2018**, *1033*, 1–34. <https://doi.org/10.1016/j.aca.2018.05.051>.
- (27) Fernández, L.; Ledezma, I.; Borrás, C.; Martínez, L. A.; Carrero, H. Horseradish Peroxidase Modified Electrode Based on a Film of Co-Al Layered Double Hydroxide Modified with Sodium Dodecylbenzenesulfonate for Determination of 2-Chlorophenol. *Sensors Actuators, B Chem.* **2013**, *182*, 625–632. <https://doi.org/10.1016/j.snb.2013.02.109>.
- (28) Veitch, N. C. Horseradish Peroxidase: A Modern View of a Classic Enzyme. *Phytochemistry* **2004**, *65* (3), 249–259. <https://doi.org/10.1016/j.phytochem.2003.10.022>.
- (29) Wang, B.; Zhang, J.; Pan, Z.; Tao, X.; Wang, H. Biosensors and Bioelectronics A Novel Hydrogen Peroxide Sensor Based on the Direct Electron Transfer of Horseradish

-
- Peroxidase Immobilized on Silica – Hydroxyapatite Hybrid Film. **2009**, 24, 1141–1145. <https://doi.org/10.1016/j.bios.2008.06.053>.
- (30) D Grieshaber. Electrochemical Biosensors - Sensor Principles and Architectures. **2008**, No. March, 1400–1458. <https://doi.org/10.3390/s80314000>.
- (31) Chu, Z.; Liu, Y.; Jin, W. Biosensors and Bioelectronics Recent Progress in Prussian Blue Films : Methods Used to Control Regular Nanostructures for Electrochemical Biosensing Applications. *Biosens. Bioelectron.* **2017**, 96 (April), 17–25. <https://doi.org/10.1016/j.bios.2017.04.036>.
- (32) Li, J.; Kuang, D.; Feng, Y. Glucose Biosensor Based on Glucose Oxidase Immobilized on a Nanofilm Composed of Mesoporous Hydroxyapatite , Titanium Dioxide , and Modified with Multi-Walled Carbon Nanotubes. **2012**, 73–80. <https://doi.org/10.1007/s00604-011-0693-1>.
- (33) Rivera-muñoz, E. M. Hydroxyapatite-Based Materials : Synthesis and Characterization. **2000**.
- (34) Petrucelli, G. C.; Kawachi, E. Y.; Kubota, L. T.; Bertran, C. A. Hydroxyapatite-Based Electrode: A New Sensor for Phosphate. *Anal. Commun.* **1996**, 33 (7), 227–229. <https://doi.org/10.1039/ac9963300227>.
- (35) Bharath, G.; Madhu, R.; Chen, S. M.; Veeramani, V.; Balamurugan, A.; Mangalaraj, D.; Viswanathan, C.; Ponpandian, N. Enzymatic Electrochemical Glucose Biosensors by Mesoporous 1D Hydroxyapatite-on-2D Reduced Graphene Oxide. *J. Mater. Chem. B* **2015**, 3 (7), 1360–1370. <https://doi.org/10.1039/c4tb01651c>.
- (36) Hench, L. L.; Wilson, J.; LeGeros, R. Z.; LeGeros, J. P. Dense Hydroxyapatite. *An Introd. to Bioceram.* **2012**, 139–180. https://doi.org/10.1142/9789814317351_0009.
- (37) White, A. A.; Best, S. M. Hydroxyapatite – Carbon Nanotube Composites for Biomedical Applications : A Review. **2007**, 13, 1–13.
- (38) Tacconi, N. R. De; Rajeshwar, K.; Lezna, R. O. Metal Hexacyanoferrates:

- Electrosynthesis, in Situ Characterization, and Applications. **2003**, 3046–3062.
- (39) Samain, L.; Grandjean, F.; Long, G. J.; Martinetto, P.; Bordet, P.; Strivay, D. Relationship between the Synthesis of Prussian Blue Pigments, Their Color, Physical Properties, and Their Behavior in Paint Layers. *J. Phys. Chem. C* **2013**, *117* (19), 9693–9712. <https://doi.org/10.1021/jp3111327>.
- (40) Velevska, J.; Pecovska-gjorgjevich, M.; Stojanov, N.; Najdoski, M. Electrochromic Properties of Prussian Blue Thin Films Prepared by Chemical Deposition Method. **2016**, *4531* (January), 380–392.
- (41) Adekunle, A. S.; Farah, A. M.; Pillay, J.; Ozoemena, K. I.; Mamba, B. B.; Agboola, B. O. Electrocatalytic Properties of Prussian Blue Nanoparticles Supported on Poly(m-Aminobenzenesulphonic Acid)-Functionalised Single-Walled Carbon Nanotubes towards the Detection of Dopamine. *Colloids Surfaces B Biointerfaces* **2012**, *95*, 186–194. <https://doi.org/10.1016/j.colsurfb.2012.02.043>.
- (42) Itaya, K.; Uchida, I.; Neff, V. D. Electrochemistry of Polynuclear Transition Metal Cyanides: Prussian Blue and Its Analogues. *Acc. Chem. Res.* **1986**, *19* (6), 162–168. <https://doi.org/10.1021/ar00126a001>.
- (43) Karyakin, A. A.; Karyakina, E. E. Electroanalytical Applications of Prussian Blue and Its Analogs. *Russ. Chem. Bull.* **2001**, *50* (10), 1811–1817. <https://doi.org/10.1023/A:1014373811238>.
- (44) Robin, B. Y. M. B.; Ronm, R. The Color and Electronic Configurations of Prussian Blue. **1962**, *1* (2), 337–342. <https://doi.org/https://doi.org/10.1021/ic50002a028>.
- (45) Piernas Muñoz, M. J.; Castillo Martínez, E. *Prussian Blue Based Batteries*; 2018. <https://doi.org/10.1007/978-3-319-91488-6>.
- (46) Hegner, F. S.; Galán-Mascarós, J. R.; López, N. A Database of the Structural and Electronic Properties of Prussian Blue, Prussian White, and Berlin Green Compounds through Density Functional Theory. *Inorg. Chem.* **2016**, *55* (24), 12851–12862.

- <https://doi.org/10.1021/acs.inorgchem.6b02200>.
- (47) Neff, V. D. Electrochemical Oxidation and Reduction of Thin Films of Prussian Blue. *J. Electrochem. Soc.* **2006**, *125* (6), 886. <https://doi.org/10.1149/1.2131575>.
- (48) Christensen, P. A.; Hamnett, A.; Higgins, S. J. A Study of Electrochemically. *J. Chem. Soc. Dalt. trans.* **1990**, 2233–2238. <https://doi.org/10.1021/acs.inorgchem.6b02200>.
- (49) Karyakin, A. A.; Karyakina, E. E. Prussian Blue-Based “artificial Peroxidase” as a Transducer for Hydrogen Peroxide Detection. Application to Biosensors. *Sensors Actuators, B Chem.* **1999**, *57* (1–3), 268–273. [https://doi.org/10.1016/S0925-4005\(99\)00154-9](https://doi.org/10.1016/S0925-4005(99)00154-9).
- (50) Karyakin, A. Chemical and Biological Sensors Based on Electroactive Inorganic Polycrystals 13.2 PROPERTIES OF TRANSITION METAL HEXACYANOFERRATES. **2008**.
- (51) TANIAI, T.; SAKURAGAWA, A.; OKUTANI, T. Fluorometric Determination of Hydrogen Peroxide in Natural Water Samples by Flow Injection Analysis with a Reaction Column of Peroxidase Immobilized onto Chitosan Beads. *Anal. Sci.* **2005**, *15* (11), 1077–1082. <https://doi.org/10.2116/analsci.15.1077>.
- (52) Rocha, F. R. P.; Ródenas-Torralba, E.; Reis, B. F.; Morales-Rubio, Á.; De La Guardia, M. A Portable and Low Cost Equipment for Flow Injection Chemiluminescence Measurements. *Talanta* **2005**, *67* (4), 673–677. <https://doi.org/10.1016/j.talanta.2005.03.021>.
- (53) Matos, R. C.; Coelho, E. O.; Souza, C. F. de; Guedes, F. A.; Matos, M. A. C. Peroxidase Immobilized on Amberlite IRA-743 Resin for on-Line Spectrophotometric Detection of Hydrogen Peroxide in Rainwater. *Talanta* **2006**, *69* (5), 1208–1214. <https://doi.org/10.1016/j.talanta.2005.12.044>.
- (54) Karyakin, A. A. Advances of Prussian Blue and Its Analogues in (Bio) Sensors. *Curr. Opin. Electrochem.* **2017**, *5* (1), 92–98. <https://doi.org/10.1016/j.coelec.2017.07.006>.

-
- (55) Liu, G.; Lin, Y. Amperometric Glucose Biosensor Based on Self-Assembling Glucose Oxidase on Carbon Nanotubes. *Electrochem. commun.* **2006**, 8 (2), 251–256. <https://doi.org/10.1016/j.elecom.2005.11.015>.
- (56) Chen, S.; Yuan, R.; Chai, Y.; Hu, F. Electrochemical Sensing of Hydrogen Peroxide Using Metal Nanoparticles: A Review. *Microchim. Acta* **2013**, 180 (1–2), 15–32. <https://doi.org/10.1007/s00604-012-0904-4>.
- (57) Richard G Compton Oxford University, U.; Eduardo Laborda Oxford University, UK & University of Murcia, S.; Kristopher R Ward Oxford University, U.; ICP. *Understanding Voltammetry : Simulation of Electrode Processes*; 2013.
- (58) Wang, J. *Analytical Electrochemistry, 2nd Edition* (Wang, Joseph); 2009. <https://doi.org/doi.org/10.1021/ed078p457.2>.
- (59) Marken, F.; Neudeck, A.; Bond, A. M. Cyclic Voltammetry. *Electroanal. Methods Guid. to Exp. Appl.* **2010**, No. d, 57–106. https://doi.org/10.1007/978-3-642-02915-8_4.
- (60) Wiley, N. Y. Allen J. Bard and Larry R. Faulkner, *Electrochemical Methods* ; 2002; Vol. 38. <https://doi.org/doi.org/10.1023/A:1021637209564>.
- (61) Elgrishi, N.; Rountree, K. J.; McCarthy, B. D.; Rountree, E. S.; Eisenhart, T. T.; Dempsey, J. L. A Practical Beginner's Guide to Cyclic Voltammetry. *J. Chem. Educ.* **2018**, 95 (2), 197–206. <https://doi.org/10.1021/acs.jchemed.7b00361>.
- (62) Autolab B.V, M. Autolab Application. Basic Overview of the Working Principle of a Potentiostat/Galvanostat (PGSTAT). **2011**, 1–3.
- (63) Sarmiento, Y. *Obtención y Caracterización de Sistemas Nanoestructurados Basados En Nanotubos de Carbono Recubiertos Con Titania, Zirconia e Hidroxiapatita*; 2011.
- (64) Gong, Z. Q.; Ngilmi, A.; Sujari, A.; Ghani, S. A. Electrochimica Acta Electrochemical Fabrication , Characterization and Application of Carboxylic Multi-Walled Carbon Nanotube Modified Composite Pencil Graphite Electrodes. *Electrochim. Acta* **2012**, 65, 257–265. <https://doi.org/10.1016/j.electacta.2012.01.057>.

-
- (65) David, I. G.; Popa, D.; Buleandra, M. Pencil Graphite Electrodes : A Versatile Tool in Electroanalysis. **2017**, 2017 (Cv).
- (66) Bowling, R.; Packard, R. T.; McCreery, R. L. Mechanism of Electrochemical Activation of Carbon Electrodes: Role of Graphite Lattice Defects. *Langmuir* **1989**, 5 (3), 683–688. <https://doi.org/10.1021/la00087a022>.
- (67) Hobbs, J. M.; Patel, N. N.; Kim, D. W.; Rugutt, J. K.; Wanekaya, A. K. Glucose Determination in Beverages Using Carbon Nanotube Modified Biosensor: An Experiment for the Undergraduate Laboratory. 8–12.
- (68) Holze, R. Piero Zanello: Inorganic Electrochemistry: Theory, Practice and Applications. *J. Solid State Electrochem.* **2006**, 10 (7), 512–513. <https://doi.org/10.1007/s10008-005-0007-9>.
- (69) Konopka, S. J.; McDuffie, B. Diffusion Coefficients of Ferri- and Ferrocyanide Ions in Aqueous Media, Using Twin-Electrode Thin-Layer Electrochemistry. *Anal. Chem.* **1970**, 42 (14), 1741–1746. <https://doi.org/10.1021/ac50160a042>.
- (70) Mukherjee, S.; Kundu, B.; Sen, S.; Chanda, A. Improved Properties of Hydroxyapatite – Carbon Nanotube Biocomposite : Mechanical , in Vitro Bioactivity and Biological Studies. **2014**, 40, 5635–5643. <https://doi.org/10.1016/j.ceramint.2013.10.158>.
- (71) Li, N. B.; Park, J. H.; Park, K.; Kwon, S. J.; Shin, H.; Kwak, J. Characterization and Electrocatalytic Properties of Prussian Blue Electrochemically Deposited on Nano-Au/PAMAM Dendrimer-Modified Gold Electrode. *Biosens. Bioelectron.* **2008**, 23 (10), 1519–1526. <https://doi.org/10.1016/j.bios.2008.01.009>.
- (72) Balasubramanian, K.; Burghard, M. Biosensors Based on Carbon Nanotubes. *Anal. Bioanal. Chem.* **2006**, 385 (3), 452–468. <https://doi.org/10.1007/s00216-006-0314-8>.
- (73) Du, D.; Wang, M.; Qin, Y.; Lin, Y. One-Step Electrochemical Deposition of Prussian Blue-Multiwalled Carbon Nanotube Nanocomposite Thin-Film: Preparation, Characterization and Evaluation for H₂O₂ Sensing. *J. Mater. Chem.* **2010**, 20 (8), 1532–

1537. <https://doi.org/10.1039/b919500a>.
- (74) Itaya, K.; Shoji, N.; Uchida, I. Catalysis of the Reduction of Molecular Oxygen to Water at Prussian Blue Modified Electrodes. *J. Am. Chem. Soc.* **1984**, *106* (12), 3423–3429. <https://doi.org/10.1021/ja00324a007>.
- (75) Liu, Y.; Chu, Z.; Jin, W. A Sensitivity-Controlled Hydrogen Peroxide Sensor Based on Self-Assembled Prussian Blue Modified Electrode. *Electrochem. commun.* **2009**, *11* (2), 484–487. <https://doi.org/10.1016/j.elecom.2008.12.029>.
- (76) You, J.; Jeong, Y. N.; Ahmed, M. S.; Kim, S. K.; Choi, H. C.; Jeon, S. Biosensors and Bioelectronics Reductive Determination of Hydrogen Peroxide with MWCNTs-Pd Nanoparticles on a Modified Glassy Carbon Electrode. *Biosens. Bioelectron.* **2011**, *26* (5), 2287–2291. <https://doi.org/10.1016/j.bios.2010.09.053>.